Combustion and Flame 161 (2014) 1–15

Contents lists available at ScienceDirect

Combustion and Flame

journal homepage: www.elsevier.com/locate/combustflame

# Uncertainty-quantification analysis of the effects of residual impurities on hydrogen–oxygen ignition in shock tubes

Javier Urzay [a,*], Nicolas Kseib [b], David F. Davidson [b], Gianluca Iaccarino [a,b], Ronald K. Hanson [b]

[a] Center for Turbulence Research, Stanford University, Stanford, CA 94305-3024, United States
[b] Mechanical Engineering Department, Stanford University, Stanford, CA 94305-3032, United States

ARTICLE INFO

*Article history:*
Received 14 April 2013
Received in revised form 14 August 2013
Accepted 15 August 2013
Available online 11 September 2013

*Keywords:*
Uncertainty quantification
Chemical kinetics
Hydrogen autoignition
Shock tubes
Supersonic combustion

ABSTRACT

This study addresses the influences of residual radical impurities on the computation and experimental determination of ignition times in $H_2/O_2$ mixtures. Particular emphasis is made on the often-times encountered problem of the presence of H-atoms in the initial composition of $H_2/O_2$ mixtures in shock tubes. Two methods are proposed for quantifying experimentally H-residual impurities in shock tubes, namely, an a priori method that consists of detecting OH traces upon shocking unfueled mixtures, and a posteriori method in which the amount of impurities is inferred by comparing fueled experimental autoignition data with calculations. A stochastic Arrhenius model that describes the amount of H-radical impurities in shock tubes is proposed on the basis of experimental measurements as a function of the test temperature. It is suggested that this statistical model yields a probability density function for the residual concentration of hydrogen radicals in standard shock tubes. Theoretical quantifications of the uncertainties induced by the impurities on autoignition times are provided by using the 5-step short chemistry of Del Álamo et al. [1]. The analysis shows that the relative effects of H-impurities on delay times above crossover become more important as the dilution increases and as the temperature and pressure decrease. Below crossover, the effects of H-impurities on the ignition delay vanish rapidly, and are negligible compared to the departures produced by the non-ideal pressure rise that is seen in some shock-tube experiments at such low temperatures. The influences of kinetic uncertainties on the ignition time are typically negligible compared to the effects of the uncertainties induced by H-impurities when the short mechanism is used, except for air at high temperatures for which kinetic uncertainties dominate. Furthermore, calculations performed with the short mechanism show that correlations between the uncertainties in the rates of branching and termination steps have only some small influences on the ignition-time variabilities near crossover, where a global sensitivity analysis shows an increasing importance of the recombining kinetics. Computational quantifications of uncertainties are carried out by using numerical simulations of homogeneous ignition subject to Monte-Carlo sampling of the concentration of impurities. For the conditions analyzed, these computations show that the variabilities produced in ignition delays by the uncertainties in H-impurities are comparable to the experimental data scatter and to the effects of typical uncertainties of the test temperature when the Stanford chemical mechanism [2] is used. The calculations also unveil that the utilization of two other different chemical mechanisms, namely San Diego [3] and GRI v3.0 [4], yields variations in the ignition delays which are within the range of the uncertainties induced by the H-impurities. Finally, the effects of residual impurities in kinetic-isolation experiments and in supersonic-combustion ramjets are briefly discussed.


## 1. Introduction

The chemistry of gaseous $H_2$–$O_2$ systems has been studied for more than half a century [5] and is of central importance as a sub-mechanism for hydrocarbon oxidation [6]. A number of $H_2$–$O_2$ detailed mechanisms have been developed [7–12,3,13–17,2,18], most of which contain about 20 or 21 elementary steps for the 8 species involved, namely $H_2$, $O_2$, $H_2O$, H, O, OH, $HO_2$ and $H_2O_2$. Reductions of these detailed mechanisms have been obtained that describe to a good extent autoignition [1,19], propagation of laminar deflagrations [20,21,19] and extinction of strained diffusion flames [22,23,19]. All these mechanisms describe the same qualitative structure of the chemical processes involved in hydrogen flames. In particular, all $H_2/O_2$ mechanisms are composed of long-period chain-branching steps, which generate a pool of active radicals. These radicals are depleted subsequently in exothermic recombination reactions. Additionally, an explosion diagram that contains

* Corresponding author.
*E-mail address:* jurzay@stanford.edu (J. Urzay).

0010-2180/$ - see front matter © 2013 The Combustion Institute. Published by Elsevier Inc. All rights reserved.
http://dx.doi.org/10.1016/j.combustflame.2013.08.012

three limits (first, second, and third explosion limits) is readily available in the literature [24] and plays a focal role in risk analysis and hazard prevention [25].

A target frequently used by chemical-kinetic modelers to obtain rate constants is the ignition delay time, which can be experimentally determined, for instance, by the use of shock tubes [26]. In shock tubes, a driver section is filled with an inert high-pressure gas separated by a diaphragm from the driven test mixture. When the diaphragm is relieved, a shock wave propagates into the driven mixture. The incident or reflected passage of the shock wave leaves the mixture at the test pressure and temperature, which eventually leads to autoignition in a mostly transport-free environment. The onset of ignition is typically characterized by a sudden rise in light emission, or by an increase on radical or product concentrations [26]. Additionally, kinetic rates can be determined by analyzing concentration time-histories through laser-absorption spectroscopy techniques if the mixture is diluted enough to isolate the reaction of interest [2]. To determine rate constants, chemical-kinetic modelers typically integrate the conservation equations for homogeneous ignition using the post-shockwave conditions as initial temperature, pressure and chemical composition [26]. There are a number of studies that have provided experimental autoignition times [27–38,4] and kinetic rates [41–44,40,39] for hydrogen by using shock tubes. Despite being much more accurate than other measuring devices, shock tubes are subject to a number of imperfections, such as non-ideal pressure rise at long times (especially below crossover), boundary-layer effects, uncertainties in the post-shock temperature, and the presence of radical impurities, the latter being analyzed in what follows.

In this paper, we use experimental, analytical and computational methods to study the effect of impurities on autoignition times for $H_2/O_2$ mixtures. A stochastic model of impurities for H radicals is proposed based on experimental data in shock tubes. Theoretical analyses based on reduced chemical descriptions are used to give a physical explanation of the influences of H-impurities on delay times, and comparisons are made with the corresponding effects of chemical-kinetic uncertainties on ignition. Additionally, numerical simulations of $H_2/O_2$ homogeneous ignition under uncertainties in the concentration of H-impurities are performed using detailed chemistry. The variabilities in the ignition time caused by uncertainties in the concentration of impurities are quantified and compared to variabilities introduced by chemical-kinetic uncertainties and by typical experimental errors in the measurements of the test temperature.

The paper is organized as follows. Section 2 shows local sensitivity studies of H-impurities in ignition-delay time calculations of relevant hydrocarbon fuels. In Section 3, methods are proposed for quantifying impurities in shock tubes by using experimental data, and a statistical model of the probability-density function (PDF) of the impurities concentration is proposed. Theoretical insight is given in Section 4 to tackle the presence of radical impurities in ignition-delay models and regime diagrams are obtained. In Section 5, Monte-Carlo sampling of the impurities PDF is performed in the numerical simulation of the ignition problem to assess the variabilities induced by the impurities in the delay time, and comparisons with experiments are performed. Sections 6 and 7 are devoted to a short assessment of the effects of impurities in kinetic-isolation experiments and supersonic combustion, respectively. Finally, conclusions are drawn in Section 8.

## 2. Sensitivity of the autoignition time of hydrocarbon fuels to radical impurities

Radical intermediates are of paramount importance for catalyzing ignition processes in combustion [45]. Residual radicals in the environment may therefore lead to significant changes in the autoignition of reacting mixtures.

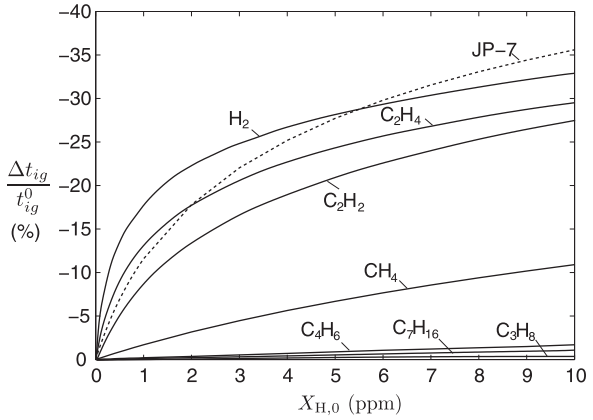


**Fig. 1.** Effects of residual H impurties on the relative autoignition time of hydrocarbon fuels (1). The ignition criterion is set as the maximum slope of the temperature time-history. The reference mechanisms are: $H_2$ [2], $C_2H_4$ [48], 2-component JP-7 surrogate [48], $C_2H_2$ [48], $CH_4$ [48], *n*-$C_7H_{16}$ [4], and $C_3H_8$ [4].

Figure 1 shows Flamemaster [46] calculations, for a number of mixtures of hydrocarbons with oxygen in typical shock-tube conditions, of the relative variations in the autoignition time $t_{ig}$,

$$\Delta t_{ig}/t^0_{ig} = \left(t_{ig} - t^0_{ig}\right)/t^0_{ig}, \tag{1}$$

produced by H-impurities. Here $t^0_{ig}$ is the nominal autoignition time calculated with the tabulated rate constants of the corresponding mechanism and zero initial H-impurities, $X_{H,0} = 0$, where the symbol $X$ denotes the molar fraction. This simple exercise shows that the ignition times of hydrogen ($H_2$), ethylene ($C_2H_4$), 2-component JP-7 surrogate and acetylene ($C_2H_2$) are influenced in a non-negligible manner by the addition of small amounts of H atoms in the initial composition. The ignition process in these fuels is dominated by an initiation period during which H atoms are formed and fed into the branching steps to generate the radical pool. As noted below, the addition of H atoms to the initial mixture can shorten this stage.

The ignition of other fuels such as butadiene ($C_4H_6$), methane ($CH_4$), propane ($C_3H_8$), and *n*-heptane (*n*-$C_7H_{16}$), is dominated by a multi-step process in which first the fuel molecule rapidly decomposes into intermediate products, which get subsequently decomposed in a slow stage and eventually lead to the exponential growth of the radical pool. For these fuels, which are mostly characterized by having a large number of hydrogen bonds, the H-impurities are rapidly scavenged by the large fuel molecules in the first decomposition stage or by the intermediate fuel products in the second decomposition period, and do not affect the autoignition time in a considerable manner.

It is therefore expected that experimental data of ignition times of $C_2H_4$, $C_2H_2$ and $H_2$ should be viewed with caution, especially in diluted conditions as shown below, unless outstanding care is taken for cleaning and maintaining high-purity conditions in the shock tube. The effects of impurities should however not play any significant role in ignition-time measurements of heavier hydrocarbons.

Special caution should be exercised with jet fuel surrogates in the present context of numerical simulations of autoignition experiments. For instance, the 2-component fuel surrogate of the partially-cracked JP-7 chosen by the HiFiRE program [47] for hydrocarbon-fueled hypersonic flight is a two-component gas-phase mixture of $C_2H_4$ and $CH_4$ (64% and 36% mole fraction, respectively), which simulates ignition, extinction and flame propagation experimental tests. The chemical mechanism required for these

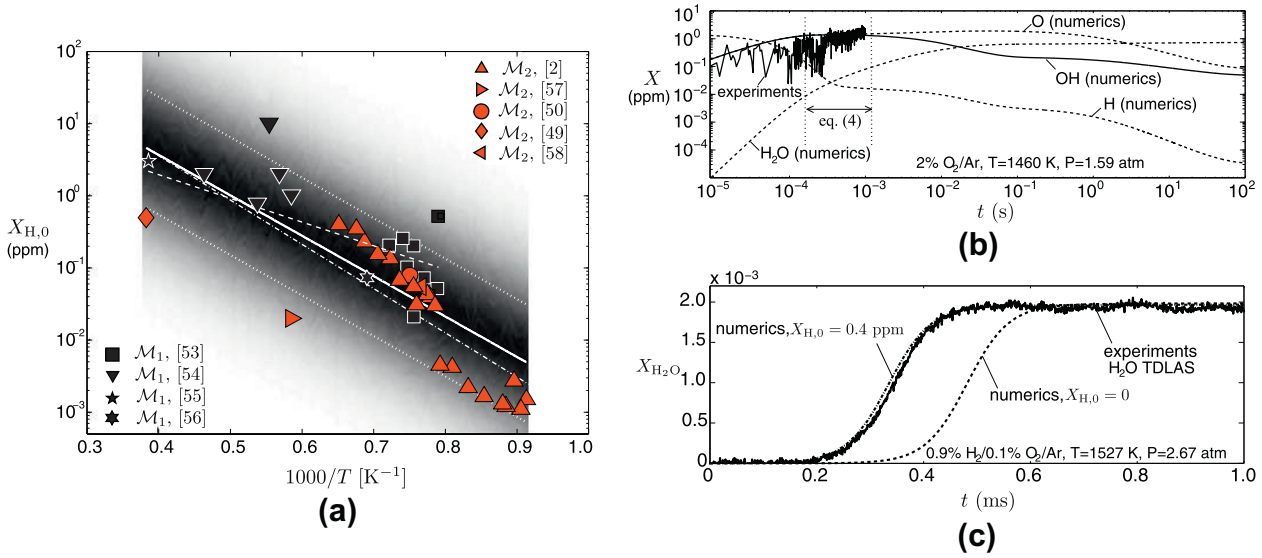


**Fig. 2.** (a) Equivalent concentration of H impurities measured in the Stanford Shock-Tube Facilities as a function of the inverse of the temperature. The shaded contours indicate the PDF of H-impurities concentration $P(X_{H,0})$ given by the stochastic model of impurities (2) and (3), with dark and white regions indicating high and low probability, respectively. The dotted lines represent one standard deviation from the linear regression curve (solid line) as given by Eq. (3). Dot-dashed and dashed lines represent linear regression models if data obtained by using either $\mathcal{M}_1$ or $\mathcal{M}_2$ are retained, respectively. (b) Example of OH laser trace [55] obtained by using the method $\mathcal{M}_1$, together with the corresponding numerical simulations of the ignition problem. (c) Example of H impurities being quantified by using method $\mathcal{M}_2$ to analyze $H_2O$ experimental traces [2] (solid line) and numerical simulations (dashed lines).

simulations must accurately describe $C_2H_4/CH_4$ oxidation over a wide range of combustion conditions. As indicated in Fig. 1, the effects of H-impurities in the autoignition of this 2-component JP-7 surrogate are non-negligible when the USC $C_2$-oxidation mechanism [48] is used, even though JP-7 is a compound made of long-chain hydrocarbons. That the autoignition time of this 2-component JP-7 surrogate is sensitive to the initial concentration of H radicals can be understood by noticing that, in its cracked version, it is mainly composed of $C_2H_4$, with the ignition delay of $C_2H_4$ being fairly sensitive to the presence of initial H radicals as evidenced in Fig. 1.

## 3. Experimental quantification of impurities in shock tubes

### 3.1. Residual impurities in shock tubes

In shock tubes, residual radicals may be generated by the decomposition of long-chained hydrocarbon molecules. These large molecules may be present in the shock tube because of three main reasons: (i) they remain in the tube as leftovers of previous experiments, (ii) they are introduced by cleaning substances for shock-tube maintenance, and (iii) they are products generated by decomposition of the organic compounds which gaskets, seals, diaphragms and wall coatings are made of. Among all sources of impurities, non-volatile compounds at room temperature, in particular heavy hydrocarbons, are most likely to be adsorbed onto surfaces and remain in the tube. To worsen the problem, these contaminants remain in the shock tube even after gas-exchange processes, ultra-vacuum pumping, and meticulous cleaning procedures [44,50,49]. These compounds act as radical precursors. As the test gas mixture is blown into the shock tube it comes in contact with the supply tubing and with the shock tube wall. Exchange with surface contaminants and with outgassing from crevices in the shock tube puts the radical precursors into the bulk gas. The diaphragm rupture and laser measurements typically occur within 1 min after filling. When the shock wave passes through the bulk gas, the high temperatures decompose the radical precursors and forms radicals such as H-atoms. Despite being supported by common experience, the above explanation is only qualitative and more research is needed in order to assess the exact causes of formation of impurities in shock tubes.

The exact composition of the impurities pool is also extremely difficult and often impractical to characterize in shock-tube normal operating conditions. However, an equivalent amount of H impurities can be inferred by using any of the following two methods proposed here: ($\mathcal{M}_1$) "a priori OH absorption in unfueled mixtures" and ($\mathcal{M}_2$) "a posteriori comparison of fueled experimental data with calculations". These two methods are described below. Experimental data obtained using these two methods are shown in Fig. 2a, in which an equivalent amount of H impurities is obtained for a range of operating temperatures in a number of shock tubes at the Shock-Tube Facilities at the High-Temperature Gasdynamic Laboratory at Stanford. Given the standardized cleaning procedures used for the operation of the Stanford Shock-Tube Facilities, the experimental results shown in Fig. 2a are most likely representative of the temperature distribution of impurities in any other typical shock tube. As depicted in Fig. 2a, the concentration of radical impurities tends to increase for increasing temperatures because of the increasingly faster activation of the radical precursors.

In a hierarchy of possible models, the results in Fig. 2a suggest a simple Arrhenius model

$$X_{H,0} = \xi \overline{X}_{H,0}, \quad \text{with} \quad \overline{X}_{H,0} = A_H e^{-T_{a,H}/T} \quad (\text{ppm}), \tag{2}$$

for the molar fraction of H-impurities $X_{H,0}$, where $T_{a,H} = 12{,}916$ K is the activation temperature and $A_H = 682.93$ ppm is a pre-exponential factor. In this formulation, $\xi$ is a dimensionless log–normal random variable given by

$$\ln \xi \sim \mathcal{N}(0, \sigma_H^2), \quad \text{with} \quad \sigma_H^2 = \frac{1}{4} \ln^2 \mathrm{UF}_H, \tag{3}$$

where $\sigma$ is the standard deviation, and $\mathrm{UF}_H$ is an uncertainty factor described below. In this analysis, the temperature $T$ is assumed to be a known parameter in the calculations. The effects of the temperature uncertainties on delay times obtained from shock-tube experiments are briefly explored in Section 5.

Eq. (2) represents a thermal-activation process for the generation of impurities, in which the nominal Arrhenius parameters $A_H$ and $T_{a,H}$ are obtained by a least-squares approximation. Eqs. (2) and (3) imply the use of a Gaussian distribution for the PDF $P(\ln X_{H,0})$, which is a model that proves to be accurate to describe the multiplicative spread of data observed at increasing temperatures. Therefore, $\ln\overline{X}_{H,0}$ represents the mean, mode and expectation of $\ln X_{H,0}$. Similarly, $\overline{X}_{H,0}$ and $\overline{X}_{H,0}exp(-\sigma_H^2)$ are the median and mode of $X_{H,0}$, respectively. The expectation of the impurities distribution is $E[X_{H,0}] = \overline{X}_{H,0}exp(\sigma_H^2/2)$, which should not be confused with $\overline{X}_{H,0}$.

In Eq. (3), a notation based on the uncertainty factor $UF_H$ has been used, which is widely employed in the assessment of chemical-kinetic uncertainties [51]. In particular, $\ln UF_H$ represents two standard deviations in $\ln X_{H,0}$ from its expectation $\ln\overline{X}_{H,0}$, which is equivalent to variations in $X_{H,0}$ within the interval $X_{H,0}/UF_H$ and $X_{H,0}UF_H$. In this model, the variance of $\ln X_{H,0}$ is constant with temperature and can therefore be written as $\mathrm{var}(\ln X_{H,0}) = \sigma_H^2$. The variance of $X_{H,0}$ is $\mathrm{var}(X_{H,0}) = \overline{X}_{H,0}^2[\exp(2\sigma_H^2) - \exp(\sigma_H^2)]$, which increases with temperature in the same manner as $\overline{X}_{H,0}^2$. Using a variance estimator for the data in Fig. 2a and Eq. (3), the uncertainty factor of the H-impurities concentration is estimated to be $UF_H \simeq 41$, which gives an expectation $E[X_{H,0}] = 5.61\overline{X}_{H,0}$.

Notice that, in general, the total amount of uncertainty in the distribution of impurities may be different from the uncertainty solely quantified by the data scatter, since each of the individual points in Fig. 1a are subject to experimental errors. However, in case of being important, these experimental errors would only increase the uncertainty factor $UF_H$. Additionally, different values of $A$, $T_{a,H}$ and $UF_H$ may be obtained depending on the data subset chosen in Fig. 2a. The present model for the PDF $P(X_{H,0})$ of the impurities concentration may be considered as a first approximation in an escalation of difficulty. Further research may be required to propose more rigorous models.

Regarding the activation process depicted in Fig. 2a. and described in Eq. (2), it may be tempting to explain the production of H impurities by arguing that they may have been generated by C–H bond breaking. Note that the C–H bond dissociation energy remains roughly of the same order of magnitude across a wide span of hydrocarbons, with a typical activation temperature of $\sim 50 \times 10^3$ K [52]. However, the H-impurities concentration $X_{H,0}$ in Fig. 5a has an activation temperature $T_{a,H} = 12{,}916$ K when data points from both $\mathcal{M}_1$ and $\mathcal{M}_2$ methods are retained for the least-squares, $T_{a,H} = 7570$ K for data points of method $\mathcal{M}_1$ only, and $T_{a,H} = 14{,}131$ K for data points of method $\mathcal{M}_2$ only. The discrepancies in the experimental activation temperatures with respect to the mean C–H bond activation temperature indicate that there may be more complex chemical processes at play and, as emphasized above, that the theory for the presence of H impurities in shock tubes outlined here is only qualitative.

### 3.2. Methods for quantifying H residual impurities in shock tubes

The two methods $\mathcal{M}_1$ and $\mathcal{M}_2$ proposed here for the experimental quantification of impurities in shock tubes are detailed in what follows.

#### 3.2.1. Method $\mathcal{M}_1$: a priori OH absorption in unfueled mixtures

In method $\mathcal{M}_1$, an $O_2$/inert gas mixture is introduced in the shock tube after cleaning but prior to any experiment with the target fuel. Then OH absorption is performed in the shock tube after passing a shock over the mixture. For these experiments, the OH absorption was performed using a laser to produce UV light of 306.7 nm wavelength. A trace of OH was found even if the mixture was thoroughly monitored to be composed of $O_2$ and inert only [53–56]. An example of an OH trace found in the experiments is shown in Fig. 2b. The resulting amounts of OH implied that a source of H radicals must have remained somewhere in the tube. In these ultra-lean conditions, the branching step $H + O_2 \leftrightharpoons OH + O$ is assumed to be the sole responsible for the early production of OH observed. The initial concentration of H can be retrieved from the intermediate plateau of the OH concentration time-history by using conservation of atoms, conservation of mass and partial equilibrium of $H + O_2 \leftrightharpoons OH + O$, which gives

$$K_1 = \frac{X_{OH}X_O}{X_H X_{O_2}} \approx \frac{2X_{OH}^2}{(X_{H,0} - X_{OH})X_{O_2,0}}. \tag{4}$$

Note that Eq. (4) is independent of the kinetic rates, and therefore method $\mathcal{M}_1$ is not influenced by any uncertainties in the chemical rates. In this formulation, $K_1 = \exp[(g_H^0 - g_{OH}^0 - g_O^0)/R^0T]$ is the equilibrium constant of $H + O_2 \leftrightharpoons OH + O$, with $R^0$ the universal gas constant and $g_i^0$ the Gibbs free energy of formation of species $i$. In Eq. (4), the approximation $X_{OH} \approx X_O$ has been made, since the initial concentration of H radicals is very small. Eq. (4) provides a relation between the concentration of OH at equilibrium, $X_{OH}$, and the initial concentration of H, $X_{H,0}$, in a given mixture of oxygen mole fraction $X_{O_2,0}$.

To illustrate this procedure, Fig. 2b shows a numerical calculation, performed with Flamemaster [46] and the reference mechanism [2], of the concentration histories for a typical mixture used in method ($\mathcal{M}_1$). Note that the OH absorption measurements can only be carried out for test times of the order of miliseconds, since the driver expansion wave and non-ideal pressure rise effects set in at longer times. During the experimental time window, the main branching step attains chemical equilibrium, which is manifested by the intermediate plateau of the OH signal. The OH concentration along this intermediate plateau is independent of the chemical rates and can be captured by using Eq. (4). Furthermore, Eq. (4) yields $X_{H,0} = X_{OH}[1 + 2X_{OH}/(X_{O_2,0}K_1)]$, which becomes $X_{H,0} \sim X_{OH}$ since $X_{OH}/(X_{O_2,0}K_1)$ is a small number at typical temperatures (of order $10^{-3}$ for the conditions in Fig. 2b). This indicates that each ppm of OH produced is approximately equal to an equivalent ppm of initial H impurities in the shock tube. The remaining branching steps reach equilibrium at a much later stage ($t > 10$ s), which is beyond the experimental range and of no interest here.

#### 3.2.2. Method $\mathcal{M}_2$: a posteriori comparison of fueled experimental data with calculations

In method $\mathcal{M}_2$, numerical calculations of autoignition are compared a posteriori with shock-tube experimental data for representative fuels, and agreement between the two is achieved after adjustment of the initial concentration of H radicals in the computations.

Typical experiments in shock tubes for kinetic isolation or autoignition use atomic absorption spectroscopy (ARAS) [26] or its more advanced tunable-diode laser version (TDLAS) for low-temperature measurements [41,44]. An example of the approach $\mathcal{M}_2$ is given in Fig. 2c, where an experimental $H_2O$ concentration time history obtained by TDLAS in a $H_2/O_2/Ar$ initial mixture [44] is matched by adding initial amounts of H in the numerical calculations. The need of adding amounts of initial H atoms in the calculations to match experimental concentration histories indicates that the shock tube must have been contaminated with impurities. A similar approach for quantifying impurities in shock tubes was adopted in other experimental studies of the same group [57,50,49,58].

## 4. Theoretical quantification of the effects of impurities in $H_2$–$O_2$ autoignition

In this section, theoretical insight is given about the physics of the interaction between radical impurities and the main test gases during the ignition process. Consideration is given here to ignition above crossover, with the below-crossover case being briefly analyzed in Section 5.2. The numeration of the chemical steps involved in the description is taken from the Stanford $H_2/O_2$ mechanism [2].

The crossover temperature $T_c$ in $H_2$–$O_2$ combustion, which increases with increasing pressure ($T_c \sim 950$ K at $p = 1$ bar), is typically defined as the limit temperature in which the main branching $H + O_2 \rightarrow OH + O$ and termination $H + O_2 + M \rightarrow HO_2 + M$ reaction rates become equal up to the multiplicative branching factor, $k_{2f}[M] = 2k_{1f}$, with $[M] = p/R^0T$ the molar concentration of the diluent gas and $R^0$ the universal gas constant. Below the atmospheric pressure, the crossover temperature indicates the second-explosion limit, in which rapid chain-branching reactions lead to the build up of active radicals that are subsequently depleted in slow exothermic recombination steps. Near the atmospheric pressure and above, the crossover temperature represents the boundary between the strong-ignition region at $T > T_c$, in which the description of the branched-chain explosions in the second limit holds to a good extent, and the weak-ignition region $T < T_c$ (yet above the third limit), in which a much slower branching path involving $HO_2$ and $H_2O_2$ leads to thermal explosion [59].

### 4.1. Reduced-order formulation

In this subsection, an extension of the description of above-crossover branched-chain explosions given in the seminal work by Del Álamo et al. [1] is made to account for non-negligible initial concentrations of residual radicals.

Following [1], for $T > T_c$ the rapid chain-branching dynamics starts with the production of H and OH radicals from collisions between $H_2$ and $O_2$ molecules through the main initiation reaction

$$\text{(13b)}\quad H_2 + O_2 \rightarrow HO_2 + H \quad \mathrm{UF}_{K,13} = 2.0,$$

(the reaction numbering follows the reference-mechanism notation hereafter [2]). The alternate chain-initiation step $H_2 + O_2 \rightarrow$ -OH + OH is not included in the reference mechanism [2] in accord with ab initio computations that relegate it to highly unlikely events. The rate constant of (13b), $k_{13b} = 0.75 \times 10^6 T^{2.43}$ exp$(-26{,}926\ \mathrm{K}/T)$ (cm$^3$ mol$^{-1}$ s$^{-1}$), was measured in earlier work [39] by a combination of O-ARAS methods in shock tube experiments and ab initio calculations. A characteristic initiation time $t_I$ associated with (13b) can be defined as $t_I = (k_{13b}[O_2]_0)^{-1}$, with the subindex $_0$ indicating initial values. In particular, $t_I$ represents the timescale over which H atoms are formed in amounts of order $[H_2]_0$. The kinetic uncertainty factor listed by Konnov [60] for this reaction is $\mathrm{UF}_{K,13} = 2.0$.

When the concentration of H radicals generated by (13b) is sufficiently large, a branched-chain process follows, which can be described by the steps

$$\text{(1f)}\quad H + O_2 \rightarrow OH + O \quad \mathrm{UF}_{K,1} = 1.1,$$
$$\text{(9f)}\quad H_2 + O \rightarrow H + OH \quad \mathrm{UF}_{K,9} = 1.3,$$
$$\text{(10f)}\quad H_2 + OH \rightarrow H_2O + H \quad \mathrm{UF}_{K,10} = 2.0,$$

[1], where (1f) and (9f) are chain-branching reactions and (10f) is a chain-propagation step. Inspection of these chemical steps shows that two H atoms are formed by (9f) and (10f) for each H atom consumed in (1f), which leads to a rapid build up of H radicals. Similar considerations can be used to describe the multiplication of OH radicals.

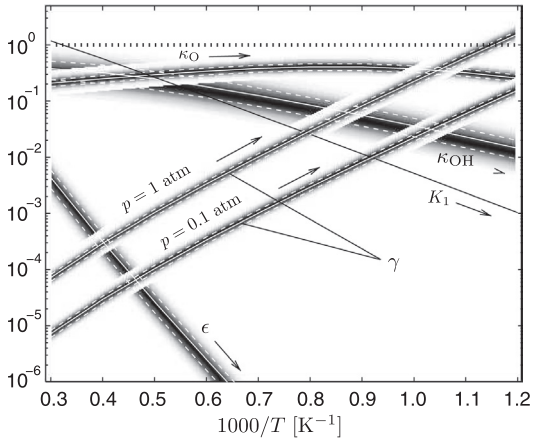


**Fig. 3.** The dimensionless parameters $\epsilon$, $\gamma$, $\kappa_O$, $\kappa_{OH}$ and $K_1$ as a function of temperature for $H_2$/air mixtures. Depicted in the figure are also the contours of the PDFs $P(\cdot)$ of each parameter that describe the variabilities on delay times induced by the uncertainties in chemical-kinetic rates when represented by the model (10) and (11). High and low probabilities are indicated by dark and white regions, respectively. Solid and dashed white lines represent mean and mean ± standard deviation, respectively.

The value of the rate constant of (1f) has been revised recently [44] by making use of advanced $H_2O$-TDLAS diagnostics, which yielded $k_{1f} = 1.04 \times 10^{14}$exp$(-7701\ \mathrm{K}/T)$ (cm$^3$ mol$^{-1}$ s$^{-1}$) within an uncertainty factor $\mathrm{UF}_{K,1} = 1.1$. A characteristic branching time $t_B$ associated with (1f) can be defined as $t_B = (2k_{1f}[O_2]_0)^{-1}$, which corresponds to the timescale over which the total number of H atoms becomes multiplied by a factor e$^1$. The values of the rate constants of (9f) and (10f) are taken from [2] as follows: $k_{9f} = !$ $3.82 \times 10^{12}$exp$(-4000\ \mathrm{K}/T) + 8.79 \times 10^{14}$exp$(-9650\ \mathrm{K}/T)$ (cm$^3$ mol$^{-1}$ s$^{-1}$) and $k_{10f} = 2.17 \times 10^8$exp$(-1740\ \mathrm{K}/T)$ (cm$^3$ mol$^{-1}$ s$^{-1}$), with uncertainty factors $\mathrm{UF}_{K,9} = 1.3$ and $\mathrm{UF}_{K,10} = 2.0$, respectively [60].

Upon induction, the radicals are depleted in direct recombination reactions (2f, 7b, 18b, 19f, 20f), which are responsible for the heat release and the corresponding temperature increment. Out of these steps, the fastest termination reaction is found to be

$$\text{(2f)}\quad H + O_2 + M \rightarrow HO_2 + M \quad \mathrm{UF}_{K,2} = 1.3,$$

where M denotes the collider. The termination step (2f) is subject to the fall-off effect, which is neglected in this study (a good approximation for not too high pressures). The rate of (2f) is taken from [2] as $k_{2f} = 6.81 \times 10^{18} T^{-1.2}$ (cm$^6$ mol$^{-2}$ s$^{-1}$) with an uncertainty factor $\mathrm{UF}_{K,2} = 1.3$ [60]. Following (2f), the $HO_2$ radical forms stable species before doing anything else and the chain is terminated. A characteristic termination time $t_T$ associated with (2f) can be defined as $t_T = (k_{2f}[M][O_2]_0)^{-1}$.

The set (13b)–(1f)–(9f)–(10f)–(2f) represents the 5-step short mechanism of Del Álamo et al. [1], the accuracy of which was tested thoroughly in earlier work (see for instance Fig. 3 in [1] or Fig. 4 below). Briefly, the 5-step mechanism is accurate in an intermediate range of temperatures, but it fails at high temperatures ($\gtrsim 2500$ K) because of the absence of dissociation reactions in the description, and at low temperatures and high pressures (near and below crossover) because it does not account for $HO_2$ and $H_2O_2$ chemistry.

When the short mechanism (13b)–(1f)–(9f)–(10f)–(2f) is used, and since the reactant consumption and the temperature increment are negligible during the induction period, the species conservation equations for the radicals become [1]

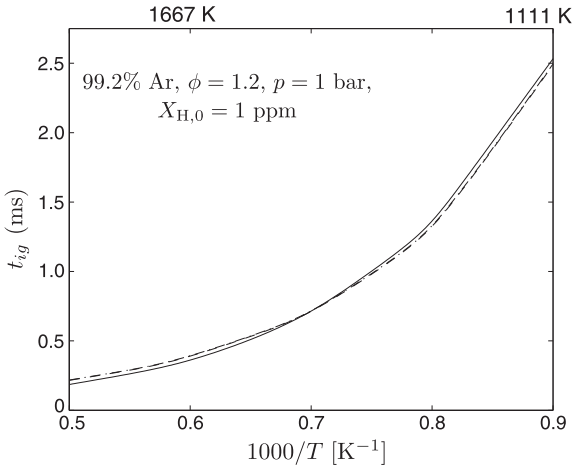


**Fig. 4.** Ignition time obtained from numerical simulations with the $H_2/O_2$ Stanford mechanism [2] (solid line), from the numerical integration of the problem (5)–(7) subject to (12) (dashed line), and from the use of formula (13) (dot-dashed line).

$$\frac{dy_H}{d\tau} = -\left(\gamma + \frac{1}{2}\right) y_H + \frac{y_O}{2} + \frac{y_{OH}}{2} + \epsilon, \tag{5}$$

$$\frac{dy_O}{d\tau} = \frac{\phi}{\kappa_O}(y_H - y_O), \tag{6}$$

$$\frac{dy_{OH}}{d\tau} = \frac{\phi}{\kappa_{OH}}(y_H + y_O - y_{OH}), \tag{7}$$

where $y_H = [H]/[H_2]_0$, $y_O = [O]/(\kappa_O[O_2]_0)$ and $y_{OH} = [OH]/(\kappa_{OH}[O_2]_0)$ are the dimensionless radical concentrations, and $\tau = t/(2k_{1f}[O_2]_0)$ is the nondimensional time. Similarly, $\kappa_{OH} = k_{1f}/k_{10f}$ and $\kappa_O = k_{1f}/k_{9f}$ are dimensionless ratios of OH and O consumption rates, respectively, and $\phi = [H_2]_0/2[O_2]_0$ is the equivalence ratio of the gaseous mixture. Note that $\kappa_O[O_2]_0$ and $\kappa_{OH}[O_2]_0$ are the characteristic steady-state concentrations of O and OH radicals, respectively. Additionally,

$$\epsilon = \frac{t_B}{t_I} = \frac{k_{13b}}{2k_{1f}}, \tag{8}$$

is the ratio of the branching-to-initiation characteristic times, and

$$\gamma = \frac{t_B}{t_T} = \frac{k_{2f}[M]}{2k_{1f}}, \tag{9}$$

is the ratio of the branching-to-termination characteristic times, which increases with increasing pressure and decreasing temperature. The value $\gamma = 1$ indicates the second explosion limit. For $\gamma > 1$, the branching dynamics is much slower than the termination, and the ignition process is utterly slow as described in earlier work [59]. For $\gamma < 1$, the branching timescale is smaller than the characteristic termination time, which rapidly leads to ignition. In the ignition zone, for $\gamma < \epsilon \ll 1$ (which occurs at high temperatures) the ordering of time scales is $t_B \ll t_I < t_T$, and for $\epsilon \ll \gamma < 1$ (which occurs at moderate-to-low temperatures) the times scales become $t_B < t_T \ll t_I$.

For illustration, the nondimensional parameters $\epsilon$, $\gamma$, $\kappa_O$ and $\kappa_{OH}$ are shown in Fig. 3 as a function of temperature and pressure. Additionally, Fig. 3 depicts the variabilities in $\epsilon$, $\gamma$, $\kappa_O$ and $\kappa_{OH}$, induced by the uncertainties in the chemical kinetic rates given by the uncertainty factors $UF_{K,1}$, $UF_{K,2}$, $UF_{K,9}$, $UF_{K,10}$ and $UF_{K,13}$. The uncertainty model

$$k_j = \eta_j \bar{k}_j, \tag{10}$$

is used for the rate constants $j$ = 1f, 2f, 9f, 10f and 13b, where $\bar{k}_j$ is the tabulated rate constant (which in turn is the median of $k_j$ and whose logarithm is the mean of $\ln k_j$), and $\eta_j$ are independent log–normal variables given by

$$\ln \eta_j \sim \mathcal{N}\left(0, \sigma_{K,j}^2\right), \quad \text{with} \quad \sigma_{K,j} = \frac{\ln UF_{K,j}}{2}. \tag{11}$$

The model (10) and (11) assumes uncorrelated uncertainties among the chemical rates, and it has been used in earlier studies of chemical-kinetic uncertainty quantification in combustion [61–63]. In particular, the model (10) and (11) and an extension of it that accounts for chemical-kinetic cross-correlations are used in Section 4.4 to compare the uncertainties in the autoignition time generated by the impurities with those produced by the uncertain chemical rates. A thorough discussion on modeling chemical-kinetic uncertainties is given in Urzay et al. [64]. A plot similar to Fig. 3 can be found in Del Álamo et al. [1] without the uncertainties induced by chemical kinetics.

Eqs. (5)–(7) are subject to the initial conditions

$$y_H = \xi_H, \quad y_{OH} = \xi_{OH} \quad \text{and} \quad y_O = \xi_O, \tag{12}$$

at $\tau = 0$, where $\xi_H = X_{H,0}/X_{H_2}$ and $X_{H,0}$ is given by the distribution (2) and (3). The initial conditions (12) were set to zero in Del Álamo's work [1], $\xi_H = \xi_O = \xi_{OH} = 0$, but they are retained here as non-zero values in order to illustrate the effect of radical impurities on the induction time.

To calculate the autoignition time, a threshold value for the radical concentrations computed from (5)–(7) and (12) needs to be specified. Here, ignition is associated with the instant in which reaction $H + O_2 \rightleftharpoons OH + O$ reaches partial equilibrium, or equivalently, when the relation $2\phi K_1/(\kappa_O\kappa_{OH}) = y_O y_{OH}/y_H$ is satisfied. In this formulation, $K_1$ is the equilibrium constant of step $H + O_2 \rightleftharpoons OH + O$, which is depicted in Fig. 3 and was used in Eq. (4) to determine the level of impurities with method $\mathcal{M}_1$. The resulting autoignition time is found not to depend much on this selection [1].

The system (5)–(7) has two complex conjugate eigenvalues with negative real parts and a real eigenvalue $\lambda_1$, which becomes positive for $\gamma < 1$ and negative for $\gamma > 1$. The solution for the autoignition time, which accounts for $\xi_H > 0, \xi_O > 0$ and $\xi_{OH} > 0$ in (12), is given by

$$t_{ig} = \frac{1}{2k_{1f}[O_2]_0\lambda_1} \ln\left(\frac{2C_{11}\phi K_1}{b_1 C_{12} C_{13} \kappa_O \kappa_{OH}}\right), \tag{13}$$

where $C_{1i}$ are the components of the $\lambda_1$-eigenvector $\mathbf{C}_1$ of the coefficient matrix in the linear system (5)–(7). Additionally, $b_1$ is a constant that depends on the initial conditions (12) and is calculated by imposing that $\mathbf{q}(\tau = 0) = \mathbf{C}^{-1}(\boldsymbol{\xi} - \mathbf{y_p})$, where $\mathbf{q} = [b_1 e^{\lambda_1 \tau}, b_2 e^{\lambda_2 \tau}, b_3 e^{\lambda_3 \tau}]^T$, $\mathbf{C}$ is the matrix of eigenvectors, $\boldsymbol{\xi} = [\xi_H, \xi_O, \xi_{OH}]^T$ is the vector of initial conditions, and $\mathbf{y}_p = [-\epsilon/(1-\gamma), -\epsilon/(1-\gamma), -2\epsilon/(1-\gamma)]$ is the particular solution of (5)–(7).

Eq. (13) is essentially the same formula as the one obtained by Del Álamo et al. [1] with the only difference that the constant $b_1$ retains here the initial conditions for the radical concentrations, which were set to zero in [1] and which play a central role here. The result obtained from formula (13) under non-zero residual impurities is shown in Fig. 4, in which the numerical integrations of the reduced problem based on short chemistry, i.e. Eqs. (5)–(7) and (12), are compared to the computations of the ignition time using Hong et al. mechanism [2] and Flamemaster.

### 4.2. Residual impurities in rich to stoichiometric mixtures above crossover

For rich to stoichiometric mixtures mixtures, $\phi \gtrsim 1$, Eqs. (5) and (6) suggest that variations in $y_O$ and $y_{OH}$ occur in a much faster time scale than the variations of $y_H$. In particular, after short dimensionless times of order $\tau \sim 1/\phi$, the information of the initial

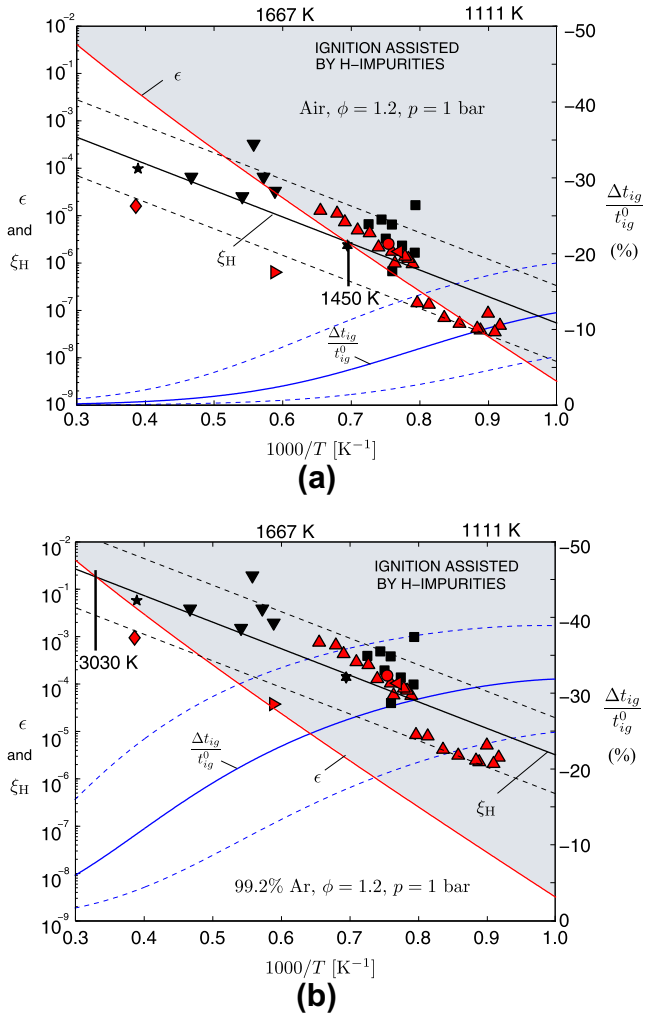


**Fig. 5.** Effects of uncertainties in the residual impurities on the autoignition time variations (1) calculated from the solution to the reduced-order ignition problem (5)–(7) subject to (12), for (a) air and (b) diluted $H_2$ mixtures after $120 \times 10^3$ samples. Solid and dashed lines indicate mean and mean ± standard deviation respectively. The symbols denote the same experimental data points shown in Fig. 2a.

concentrations $\xi_O$ and $\xi_{OH}$ is lost and the O and OH atoms reach steady state with $y_H \sim y_O$ and $y_{OH} \sim 2y_H$. In this limit, Eq. (4) can be integrated to give the time evolution of the concentration $y_H$. For $t_{ig}/t_B \gg 1 \gtrsim 1/\phi$, the ignition time

$$t_{ig,R} \simeq \frac{1}{2k_{1f}[O_2]_0(1-\gamma)} \ln\left\{\frac{\phi K_1}{\kappa_O \kappa_{OH}[\xi_H + \epsilon/(1-\gamma)]}\right\}, \tag{14}$$

is obtained. As pointed out in Del Álamo et al. [1], the validity of Eq. (14) extends from rich mixtures $\phi \gg 1$ to near stoichiometric mixtures $\phi \sim 1$. In view of Eq. (14), a competition occurs between the kinetic parameter $\epsilon/(1-\gamma)$ and the dimensionless concentration of impurities $\xi_H$. The H-impurities become important if

$$\xi_H \gtrsim \epsilon/(1-\gamma), \tag{15}$$

or equivalently, if

$$X_{H,0}/t_B \gtrsim k_{13b} X_{H_2,0} X_{O_2,0} p/(R^0 T), \tag{16}$$

which corresponds to the limit in which the molar fraction of the H-impurities is larger than the molar fraction of H atoms generated by the initiation step (13b) during a characteristic branching time $t_B$.

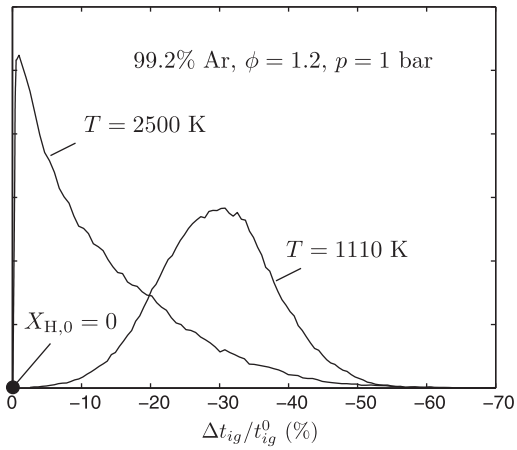


**Fig. 6.** PDFs of the autoignition time variations $P(\Delta t_{ig}/t^0_{ig})$ as defined in (1) calculated from the solution of the reduced-order ignition problem (5)–(7) subject to (12), and integrated using 10,000 samples of the impurities concentration for each temperature value.

Furthermore, Eq. (14) shows that the autoignition time is bounded by the upper limit $t^0_{ig,R}$, in that $t_{ig,R}$ is always smaller than $t^0_{ig,R}$ if impurities are present, with $t_{ig,R}$ tending to $t^0_{ig,R}$ from the left as $\xi_H \to 0$.

Based on the criterion (15), Fig. 5(a) and (b) shows the temperature dependence of the dimensionless parameters $\epsilon$ and $\xi_H$ as well as the autoignition-time decrement caused by H-impurities, for both diluted and non-diluted conditions. In particular, it is observed that dilution increases the relevance of the H-impurities, in that the effective value of $\xi_H$ in (15) increases with increasing dilution because of the decrease in $X_{H_2}$. The effects of the H-impurities increase as the temperature decrease (still above crossover) because of the disparity in the slopes of $\epsilon$ and $\xi_H$, which makes the initiation (13b) to become slower at a faster rate than the decrease in the speed of the activation process that leads to the generation of H impurities from the radical precursors. The effects of the H-impurities are largely independent of the pressure for moderately to high temperatures, for which $\gamma \ll 1$, but at low temperatures $\gamma \simeq 1$ an increase in pressure causes a faster termination rate, which in turn reduces the effects of contamination of the shock tube on the delay time. Overall, autoignition-time decrements of order 15% for air, and of order 30% for 99.2%-Ar diluted mixtures are predicted by this model in the low-temperature end, with increasing variance and increasing departures from the nominal autoignition time $t^0_{ig}$ as the temperature decreases. These estimates are consistent with the findings shown in Section 5 where the full mechanism is used for calculations.

Fig. 6 shows the autoignition-time PDFs obtained by sampling the problem (5)–(7) and (12) subject to the impurities distribution (2) and (3). It is observed that the PDFs transit from lognormal to near-normal as the temperature decreases, a phenomenon which is explained below.

In the limit in which the amount of impurities is – with high probabilities – very small compared to the amount of H atoms generated by the initiation step (13b) during a characteristic branching time, $P[\xi_H \ll \epsilon/(1-\gamma)] \to 1$, which typically occurs at high temperatures, a series expansion of (14) gives

$$t_{ig,R} = t^0_{ig,R} - \frac{1}{2k_{1f}[O_2]_0(1-\gamma)}\left\{\left(\frac{(1-\gamma)\xi_H}{\epsilon}\right) + O\left[\left(\frac{(1-\gamma)\xi_H}{\epsilon}\right)^2\right]\right\}, \tag{17}$$

Eq. (17) shows that, in this limit, the ignition-time decrement is log–normally distributed to second order in $(1-\gamma)\xi_H/\epsilon$ if the model for H-impurities (2) and (3) is used, with expectation and variance given by

$$\mathrm{E}[t_{ig,R}] \simeq t^0_{ig,R} - \frac{1}{2k_{1f}[\mathrm{O}_2]_0}\left(\frac{\mathrm{E}[\xi_H]}{\epsilon}\right), \tag{18}$$

and

$$\mathrm{var}[t_{ig,R}] \simeq \frac{1}{4k^2_{1f}[\mathrm{O}_2]^2_0}\left(\frac{\mathrm{var}[\xi_H]}{\epsilon^2}\right), \tag{19}$$

where $\mathrm{E}[\xi_H] = \mathrm{e}^{\sigma_H^2/2}\overline{\xi}_H$, $\mathrm{var}[\xi_H] = (\mathrm{e}^{2\sigma_H^2} - \mathrm{e}^{\sigma_H^2})\overline{\xi}^2_H$, $\overline{\xi}_H = \overline{X}_{H,0}/X_{H_2,0}$ and $\sigma_H$ is given in (3). Eqs. (18) and (19) state the linearity between the mean and variance of the autoignition time and the impurities, and in particular, they reveal that both the mean deviation from the nominal autoignition time $t^0_{ig,R} - \mathrm{E}[t_{ig,R}]$ and its variance $\mathrm{var}[t_{ig,R}]$ increase with decreasing temperature, as shown in Fig. 5.

In the opposite limit, namely the limit in which the amount of impurities is -with high probabilities- very large compared to the amount of H atoms generated by the initiation step (13b) during a characteristic branching time, $P[\xi_H \gg \epsilon/(1-\gamma)] \to 1$, which typically occurs at low temperatures (still above crossover), the ignition delay asymptotes to

$$t_{ig,R} = \frac{1}{2k_{1f}[\mathrm{O}_2]_0(1-\gamma)}\left\{\ln\left(\frac{\phi K_1}{\kappa_O\kappa_{OH}\xi_H}\right) - \left(\frac{\epsilon}{\xi_H}\right) + O\left[\left(\frac{\epsilon}{\xi_H}\right)^2\right]\right\}. \tag{20}$$

The leading-order approximation in (20) predicts a Gaussian distribution for $t_{ig,R}$ if the model for H-impurities (2) and (3) is used, which contradicts the physical constraint that $t_{ig,R} < t^0_{ig,R}$. To compensate for this, the second approximation in (20), has a lognormal distribution that sweeps out the high-$t_{ig,R}$ tail of the leading-order Gaussian distribution. The resulting distribution of $t_{ig,R}$ has a distribution with expectation and variance given by

$$\mathrm{E}[t_{ig,R}] \simeq t^0_{ig,R} - \frac{1}{2k_{1f}[\mathrm{O}_2]_0(1-\gamma)}\left\{\ln\left[\frac{(1-\gamma)}{\epsilon}\right] + \mathrm{E}[\ln\xi_H] + \epsilon\mathrm{E}\left[\frac{1}{\xi_H}\right]\right\}, \tag{21}$$

and

$$\mathrm{var}[t_{ig,R}] \simeq \frac{1}{4k^2_{1f}[\mathrm{O}_2]^2_0(1-\gamma)^2}\left\{\mathrm{var}[\ln\xi_H] + \epsilon^2\mathrm{var}\left[\frac{1}{\xi_H}\right]\right\}, \tag{22}$$

where $\mathrm{E}[\ln\xi_H] = \ln\overline{\xi}_H$, $\mathrm{E}[1/\xi_H] = \mathrm{e}^{\sigma_H^2/2}/\overline{\xi}_H$, $\mathrm{var}[\ln\xi_H] = \sigma^2_H$, $\mathrm{var}[1/\xi_H] = (\mathrm{e}^{2\sigma_H^2} - \mathrm{e}^{\sigma_H^2})/\overline{\xi}^2_H$, $\overline{\xi}_H = \overline{X}_{H,0}/X_{H_2,0}$ and $\sigma_H$ is given in (3). Eq. (21) indicate an intricate temperature dependence of the variance $\mathrm{var}[t_{ig,R}]$ and mean deviation $t^0_{ig,R} - \mathrm{E}[t_{ig,R}]$.

### 4.3. Residual impurities in lean mixtures above crossover

In practical applications for high-speed propulsion, in which a hydrogen stream is ignited by a hot coflow, autoignition tends to occur in lean conditions [84]. For lean mixtures $\phi \ll 1$, Eqs. (5)–(7) indicate that the variations in $y_H$ occur much faster than the variations in $y_O$ and $y_{OH}$. In particular, after short dimensionless times of order $\tau \sim \phi$, the information in the initial condition $\xi_H$ is lost and H reaches steady state, with $y_H = (y_O/2 + y_{OH}/2 + \epsilon)/(\gamma + 1/2)$. Upon substituting this result in (6) and (7) and solving the resulting linear system, the formula

$$t_{ig,L} \simeq \frac{1}{[\mathrm{H}_2]_0\sqrt{2k_{9f}k_{10f}}} \times \ln\left\{\left(\frac{2\phi K_1}{k_O k_{OH}}\right)\frac{1+\sqrt{\frac{2k_O}{k_{OH}}}}{\left[\left(2+\sqrt{\frac{2k_O}{k_{OH}}}\right)\left(\frac{\epsilon}{2}\right) + \left(\xi_O + \frac{\xi_{OH}}{2}\right)\right]}\right\}, \tag{23}$$

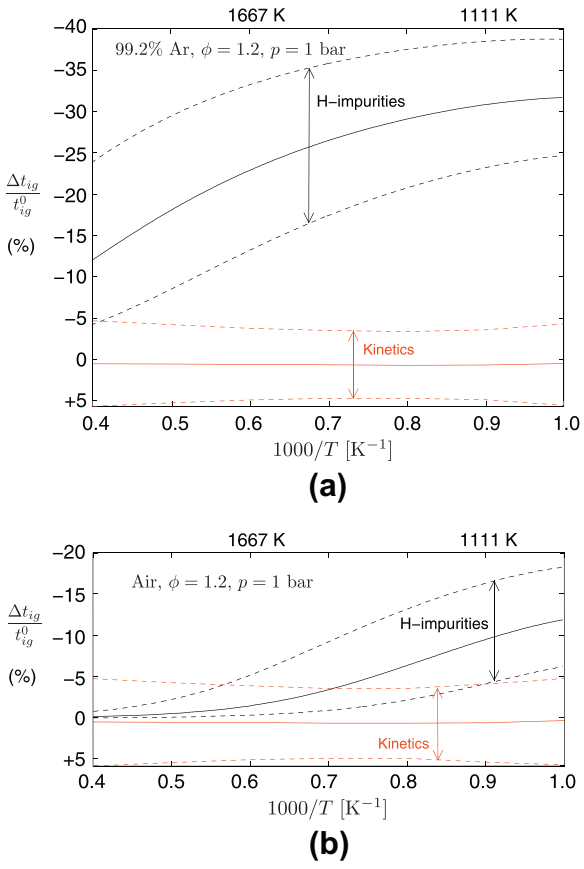


**Fig. 7.** Mean (solid lines) and mean ± standard deviation (dashed lines) of the autoignition time variation (1) as a function of temperature after $120 \times 10^3$ samples, for (a) diluted and (b) air mixtures with $H_2$. The figure shows the comparative effect of the chemical-kinetic uncertainties (red color online) and the uncertainties in the concentration of H-impurities (black color).

for the ignition delay is obtained, which is valid in the limit $t_{ig}/t_B \gg 1 \gg \phi$ and $\gamma \ll 1$. Eq. (23) implies that the effects of OH impurities in the system become non-negligible if

$$X_{OH,0}/t_L \gtrsim k_{13b}X_{H_2,0}X_{O_2,0}p/(\mathrm{R}^0T), \tag{24}$$

or equivalently, if the molar fraction of OH impurities is larger than the molar fraction of OH atoms generated by the initiation step (13b) (note that the H atoms are consumed very fast by step (1f)) during a characteristic branching time $t_L = 1/([\mathrm{H}_2]_0\sqrt{k_{9f}k_{10f}})$. The ratio of the critical amount of H-impurities, given by (16) to the critical amount of OH-impurities, given by (24), is $X_{H,0}/X_{OH,0} \sim t_B/t_L = \phi(\kappa_O\kappa_{OH})^{-1/2}$, which indicates that ppm-levels of OH-impurities suffice to perturb considerably the ignition delay if the mixture is sufficiently lean, $\phi \lesssim (\kappa_O\kappa_{OH})^{1/2} = O(10^{-1})$.

A more general expression for $t_{ig}$ that likely bridges the rich to stoichiometric region $\phi \gtrsim 1$ and lean $\phi \ll 1$ regions can be obtained, across which the effects of all impurities H,OH and O become important, but the derivation of this formula will not be pursued here.

### 4.4. Effects of chemical-kinetic uncertainties on ignition times

The results in Fig. 5 are compared here with Fig. 7, which shows the effects of the uncertainties in the chemical-kinetic rates on $t_{ig}$. Here, the uncertainties in the chemical-kinetic rates are imposed by the uncertainty factors in (1f), (2f), (9f), (10f) and (13b)

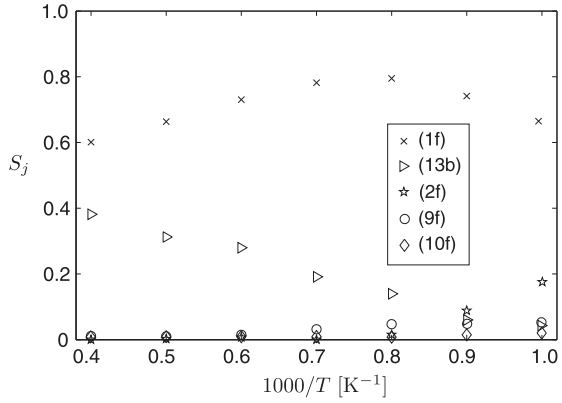


**Fig. 8.** Global sensitivities (25) of the ignition time to the chemical rates as a function of temperature. Here the ignition time is calculated from the solution of the reduced-order ignition problem (5)–(7) subject to (12) with $\xi_H = \xi_{OH} = \xi_O = 0$.

described above, and by using the uncertainty model (10) and (11) for the rate constants upon integrating the problem (5)–(7) subject to $\xi_H = \xi_{OH} = \xi_O = 0$. In particular, it is observed from Fig. 7 that, according to the 5-step short mechanism, the uncertainties induced by the chemical kinetics on $t_{ig}$ are typically smaller than the uncertainties induced by the H-impurities, except for air at high temperatures ($T \gtrsim 1600$ K) at which kinetic uncertainties dominate.

To ascertain which steps contribute significantly to the chemical-kinetic uncertainty in $t_{ig}$, the global sensitivities

$$S_j = \mathrm{var}\{\mathrm{E}[t_{ig}|k_j]\}/\mathrm{var}[t_{ig}], \tag{25}$$

are calculated for $j$ = 1f, 2f, 9f, 10f and 13b as a function of the temperature. In particular, $S_j$ is a number that is comprised between 0 and 1 by the total law of variance, with $S_j = 0$ representing no sensitivity to $k_j$, and $S_j = 1$ indicating full sensitivity to $k_j$ in that the variance of $t_{ig}$ can be explained by only the variance in the uncertain rate constant $k_j$.

Notice that (25) is a much better measure of the sensitivity than local sensitivities based on partial derivatives $\partial t_{ig}/\partial k_j$, since the latter do not account for the extent and nature of the variation of $k_j$. In particular, approximate values of the global sensitivities (25) can be obtained by using a first-order polynomial-chaos expansion for $t_{ig}$ as a function of the random variables $\eta_j$ given in (11). This procedure yields the approximated result

$$S_j \simeq \frac{\left(\sum_{m=1}^{N} t_{ig,m}\beta_{j,m}\right)^2}{\sigma_{K,j}^2 N^2 \mathrm{var}[t_{ig}]}, \tag{26}$$

with $\sigma_{K,j}$ given in (11) and $N$ being the number of samples per temperature value. The derivation of Eq. (26) is shown in Appendix A. Fig. 8 shows the global sensitivities calculated using (26), which indicate that the branching (1f) and – in a lesser extent – initiation (13b) steps are the most relevant steps for this problem. The termination step (2f) only becomes important at low temperatures near crossover.

When the chemical-kinetic uncertainties are modeled by using (10) and (11), the resulting mean of the autoignition time is longer than the nominal $t_{ig}^0$, which is based on the tabulated values of the rate constants $\bar{k}_j$. This effect can be explained by using Eq. (17), by which the ignition time becomes

$$t_{ig} \simeq \frac{1}{2\bar{k}_{1f}[\mathrm{O}_2]_0(\eta_1 - \bar{\gamma}\eta_2)} \ln\left(\frac{\eta_1 - \bar{\gamma}\eta_2}{\bar{\epsilon}\eta_{13}}\right), \tag{27}$$

up to small deterministic constants, and where $\epsilon = \bar{k}_{13b}/2\bar{k}_{1f}$ and $\bar{\gamma} = \bar{k}_{2f}[\mathrm{M}]/2\bar{k}_{1f}$. The retention of only $\eta_1$,$\eta_2$ and $\eta_{13}$ as random

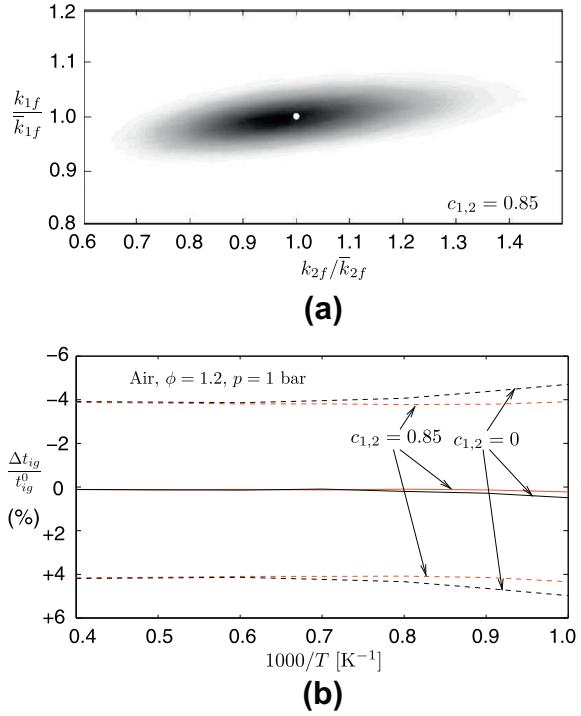


**Fig. 9.** (a) Joint PDF of the rates $k_{1f}$ and $k_{2f}$ according to the uncertainty model (30) and (31), with dark and white zones indicating high and low probability, respectively. (b) Mean (solid lines) and mean ± standard deviation (dashed lines) of the autoignition time variation (1) in a $H_2$/air mixture calculated from the solution to the reduced-order ignition problem (5)–(7) subject to (12) with $\xi_H = \xi_{OH} = \xi_O = 0$, for correlated (red color online, $120 \times 10^3$) and uncorrelated (black color) branching (1f) and termination (2f) rates after $120 \times 10^3$ samples.

variables is justified on the basis of the global sensitivities calculated in Fig. 8. Sufficiently far above from crossover, $\bar{\gamma} \ll (\mathrm{UF}_{K,1}\mathrm{UF}_{K,2})^{-1}$ and $\bar{\epsilon} \ll (\mathrm{UF}_{K,1}\mathrm{UF}_{K,13})^{-1}$, and therefore (27) becomes

$$t_{ig} \simeq \frac{1}{2\bar{k}_{1f}[\mathrm{O}_2]_0\eta_1} \ln\left(\frac{1}{\bar{\epsilon}}\right). \tag{28}$$

In view of the high-temperature limit (28), it is clear that the ignition time has a lognormal distribution with the tail pointing towards the slow side and with an expectation given by

$$\mathrm{E}[t_{ig}] \simeq \frac{\mathrm{e}^{\sigma_{K,1}^2/2}}{2\bar{k}_{1f}[\mathrm{O}_2]_0} \ln\left(\frac{1}{\bar{\epsilon}}\right), \tag{29}$$

which is larger than the corresponding nominal ignition time $t_{ig}^0 \simeq (2\bar{k}_{1f}[\mathrm{O}_2]_0)^{-1}\ln(1/\bar{\epsilon})$ by a factor of 1%, as observed in Fig. 7. Similarly, the variance of the autoignition time variation in (1) becomes $\exp(2\sigma_{K,1}^2) - \exp(\sigma_{K,1}^2) \sim 2.2\%$, also in agreement with Fig. 7. These considerations highlight the importance of accurate measurements of the branching rate (1f) to calculate ignition times [2].

Earlier experimental work [44] determined the rate constant $k_{1f}$ within a kinetic uncertainty factor $\mathrm{UF}_{K,1} = 1.1$ by using $H_2O$-TDLAS diagnostics, in which $k_{1f}$ was fitted to match the maximum slope of the experimental $H_2O$ profile. However, it was also remarked there that the maximum slope of the experimental $H_2O$ profile becomes sensitive to the rate $k_{2f}$ at low temperatures near crossover (see Fig. 2 in Ref. [44]), which indicates a potential cross-correlation among the errors in the measurements of $k_{1f}$ and $k_{2f}$. This cross-correlation is not included in the uncertainty model (10) and (11) nor in the kinetic uncertainty factors $\mathrm{UF}_{Kj}$. To test the effects of a cross-correlation between the uncertainties in the branching

(1f) and termination (2f) rates, calculations are performed by using the uncertainty models

$$k_{1f} = \left(\eta_1^{\sqrt{1-c_{1,2}^2}}\right)\left(\eta_2^{\frac{c_{1,2}\sigma_{K,1}}{\sigma_{K,2}}}\right)\bar{k}_{1f}, \tag{30}$$

$$k_{2f} = \eta_2 \bar{k}_{2f}, \tag{31}$$

with the remaining three rates being kept fixed to their tabulated values from [2], i.e. $k_{9f} = \bar{k}_{9f}, k_{10f} = \bar{k}_{10f}$ and $k_{13b} = \bar{k}_{13b}$. In this formulation, $\eta_1$ and $\eta_2$ are log–normal independent variables given by (11). Additionally, $c_{1,2}$ is the correlation coefficient between ln $k_{1f}$ and ln $k_{2f}$, the exact quantification of which remains unknown in the literature to the best knowledge of the authors. Note that the exponents of $\eta_1$ and $\eta_2$ in (30) and (31) are chosen in a way to triangularize the covariance matrix of the logarithm of the rate vectors. In this way, the quantities $k_{1f}$ and $k_{2f}$ form a joint bivariate lognormal distribution in the basis $\{\ln\eta_1, \ln\eta_2\}$, as shown in Fig. 9a.

Figure 9b shows that effects of a high branching-termination correlation, $c_{1,2} = 0.85$, are mostly negligible for autoignition, with only a secondary influence in $t_{ig}$ near crossover, where the branching and termination time scales start becoming comparable. These results are consistent with Eq. (27), which predicts that $t_{ig}$ is mostly independent of the termination time scale except for low temperatures ($\bar{\gamma} = 0.32$ in the low-temperature end of Fig. 9b).

## 5. Computational quantification of the effects of impurities in $H_2$–$O_2$ ignition

In this section, numerical simulations with Flamemaster [46] are performed to integrate the accumulation–reaction conservation equations with detailed $H_2/O_2$ chemistry under uncertainties in H-impurities, and comparisons are made with experimental data. The calculations are carried out for conditions above and below crossover. The detailed kinetics used in the computations is the Stanford $H_2/O_2$ chemical mechanism of Hong et al. [2], but also the San Diego [3] and GRI v3.0 [4] kinetic descriptions are used for comparisons.

In all the computations shown below, a characteristic error in the test temperature $\Delta T = 10$ K has been included, the reason being that in shock tubes the post-shock temperature is estimated by substituting in the Rankine–Hugoniot equations the shock speed, which is obtained by a procedure that involves the detection of the shock by pressure transducers and the differentiation of its position in time, giving errors of order 10 K in the temperature. Further details are given elsewhere [54]. As shown below, this uncertainty in the temperature produces non-negligible uncertainties in the ignition time, which are comparable to the uncertainties induced by impurities and to the variabilities obtained by using two other chemical mechanisms.

### 5.1. Computations of $H_2/O_2$ ignition subject to impurities above crossover

Figures (10) and (11) show comparisons of the computations of ignition under uncertainties in the H-impurities with experimental data of Bhaskaran et al. [36] for air, and of Petersen et al. [37] for diluted mixtures. In these calculations, the uncertainty model (2) and (3) has been used for the H-impurities. It is worth noticing that for the air case in Fig. 10, the effect of the temperature uncertainty, the variabilities among different mechanisms and the uncertainties induced by the impurities are all within the same range with regard to their effects on the ignition time. This is not the case for the diluted mixture in Fig. 11, for which the uncertainties in $t_{ig}$ induced by the impurities tend to dominate everything else.

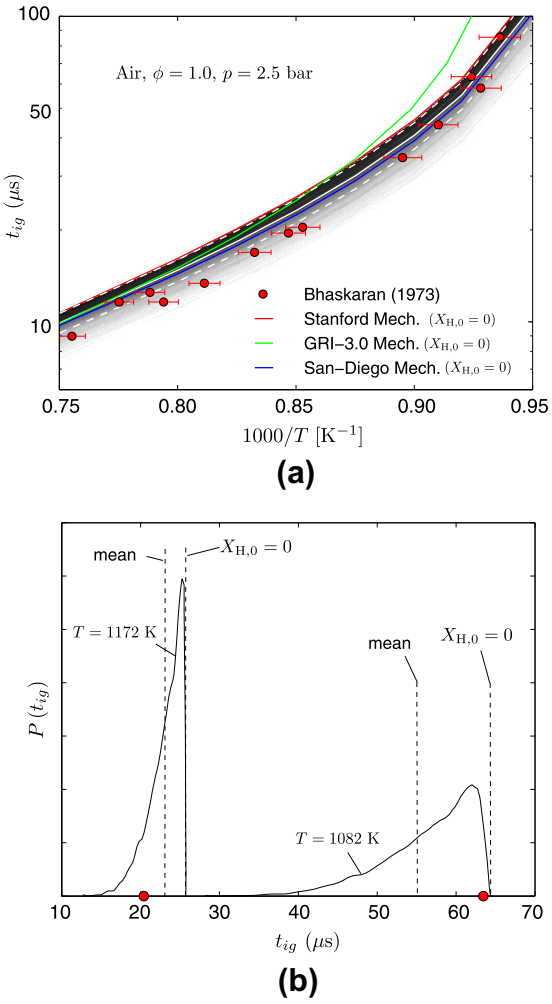


**Fig. 10.** (a) Contours of the PDF of the ignition time $P(t_{ig})$ for $H_2$/air mixtures after $2 \times 10^5$ samples of the concentration of H-impurities, calculated using the Stanford mechanism [2], together with Bhaskaran et al. experiments [36] (red dots), with darker regions indicating high probability. Panel (a) shows 1% error bars in temperature around experimental points, the mean E[$t_{ig}$] (solid white line), E[$t_{ig}$] ± standard deviation (dashed white line), and deterministic calculations of $t_{ig}$ calculated with $X_{H,0} = 0$ using the Stanford mechanism (red solid line) [2], the San Diego mechanism (blue solid line) [3] and the GRI v3.0 mechanism (green solid line) [4]. Panel (b) shows scaled PDFs $P(t_{ig})$ at two different temperatures for the same pressure and mixture composition as in (a), with dots (red color online) indicating experimental data at the corresponding temperature.

In these calculations, the global trends shown by the theoretical analyses in Section 4 are confirmed, in that the diluted case in Fig. 11b shows a wider PDF of $t_{ig}$ than in the air case, and the PDF transits from lognormal to a 'nearly-Gaussian' distribution as temperature decreases (still above crossover), as predicted by the theory.

Additionally, Fig. 12 shows that the variance var[$t_{ig}$] and mean deviation E[$t_{ig}$] – $t_{ig}^0$ increase as the temperature decreases until crossover is reached. Below crossover, both magnitudes decay rapidly with decreasing temperatures. The effects of H impurities below crossover are negligible. Note that the theoretical model in Section 4 and the original impurity-less formulation of Del Álamo [1] do not include the chemistry near crossover, and therefore this effect could not be captured. The reasoning behind the vanishing effect of H impurities below crossover is explained in what follows.

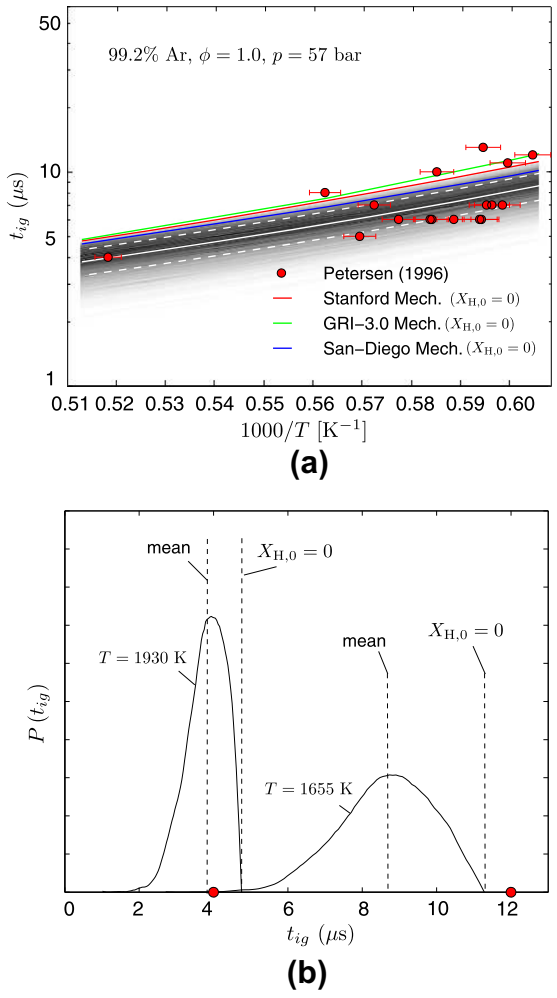


**Fig. 11.** (a) Contours of the PDF of the ignition time $P(t_{ig})$ for a $H_2/O_2$ mixture diluted with Ar after $2 \times 10^5$ samples of the concentration of H-impurities, calculated using the Stanford mechanism [2], together with Petersen et al. experiments [37] (red dots), with darker regions indicating high probability. Panel (a) shows 1% error bars in temperature around experimental points, the mean $E[t_{ig}]$ (solid white line), $E[t_{ig}]$ ± standard deviation (dashed white line), and deterministic calculations of $t_{ig}$ calculated with $X_{H,0} = 0$ using the Stanford mechanism (red solid line) [2], the San Diego mechanism (blue solid line) [3] and the GRI v3.0 mechanism (green solid line) [4]. Panel (b) shows scaled PDFs $P(t_{ig})$ at two different temperatures for the same pressure and mixture composition as in (a), with dots (red color online) indicating experimental data at the corresponding temperature.

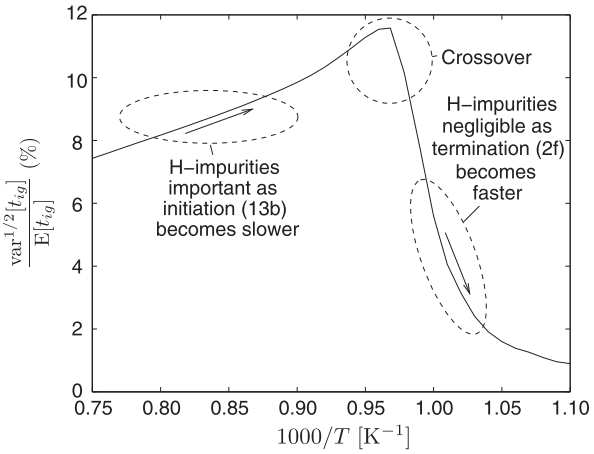


**Fig. 12.** Dimensionless standard deviation induced by the uncertainties in H-impurities on the ignition time calculated using the Stanford mechanism [2] after $2 \times 10^5$ samples, for $H_2$/air, $\phi = 1.0$ and $p = 2.5$ bar. The mean deviation $E[t_{ig}] - t_{ig}^0$ follows a similar trend with decreasing temperature as the standard deviation shown here.

### 5.2. Computations of $H_2/O_2$ ignition subject to impurities below crossover

At temperatures below crossover, the parameter $\gamma$ in (9) is $\gamma > 1$, indicating that the branching step (1f) is slower than the termination reaction (2f). Therefore, all radicals tend to be removed rapidly by (2f) with a time constant that decreases with decreasing temperature and increasing pressure. Below crossover, $\gamma > 1$, the ordering of time scales becomes $t_T < t_B \ll t_I$. In Treviño's [65] description of ignition below crossover, the step (2f) generates $HO_2$ upon removing H radicals. The resulting $HO_2$ forms $H_2O_2$ through the steps (6f) $HO_2 + HO_2 \rightarrow H_2O_2 + O_2$ and (15b) $HO_2 + H_2 \rightarrow H_2O_2 + H$, with $UF_{K,6} = 2.5$ and $UF_{K,15} = 3.0$, respectively [60]. The $H_2O_2$ is subsequently depleted in the exothermic reaction (3f) $H_2O_2 + M \rightarrow OH + OH + M$, with $UF_{K,3} = 1.2$ [2].

The slowest step among (13b)–(1f)–(9f)–(10f)–(2f)–(6f)–(15b)–(3f) at low temperatures tends to be (3f), which sets the ignition time in the first approximation, with $HO_2$ being approximately in steady state [59]. Because of the rapid removal of radicals by the fast termination step (2f), the H-impurities play a very modest role in ignition below crossover, as confirmed in the calculations shown in Figs. 12 and 13.

The long test times make measurements of ignition times below crossover particularly difficult for a number of reasons, among which the most important one seems to be the non-ideal pressure-rise in the shock tube during the experimental time window [26]. An interesting question is whether the impurities in shock tubes may have comparable effects to the shift in the ignition time caused by non-ideal pressure rise. Although the computations in Fig. 13a show some effect of impurities in the near-crossover region in the $H_2$–air experiments of Bhaskaran et al. [36], these experiments did not fully reach below-crossover temperatures. On the other hand, Fig. 13b concludes that the effects of H-impurities below crossover in the highly diluted mixture of Petersen et al. [37] are practically negligible compared to non-ideal effects, which would otherwise lead to the prediction of much shorter autoignition times in accord with experiments if, for instance, other software such as CHEMSHOCK is used to model the pressure variations in the shock tube [66].

## 6. Residual impurities in kinetic-isolation experiments

A short comment must be made here about the possible influences of residual impurities in the determination of kinetic rates based on shock-tube data. Kinetic-isolation experiments are aimed at isolating the value of rate constants of chemical mechanisms. However, the determination of the value of the target rate constant typically relies on the remaining rate constants of the mechanism and on the degree of certainty in the values of composition and temperature. For instance, in Hong et al. experiments [44], the slope of the $H_2O$ profile is most sensitive to the rate constant of the branching step (1f) and – in a lesser extent – to the termination step (2f) (the latter becoming increasingly important at near-crossover temperatures as emphasized in Section 4.4), but it remains mostly insensitive to the level of impurities in the shock tube and to the remaining rates in the $H_2/O_2$ mechanism.

Therefore, in Hong et al. experiments [44] only a weak correlation is expected between the uncertainties in the concentration of impurities and the rate constant of the branching step (1f), and

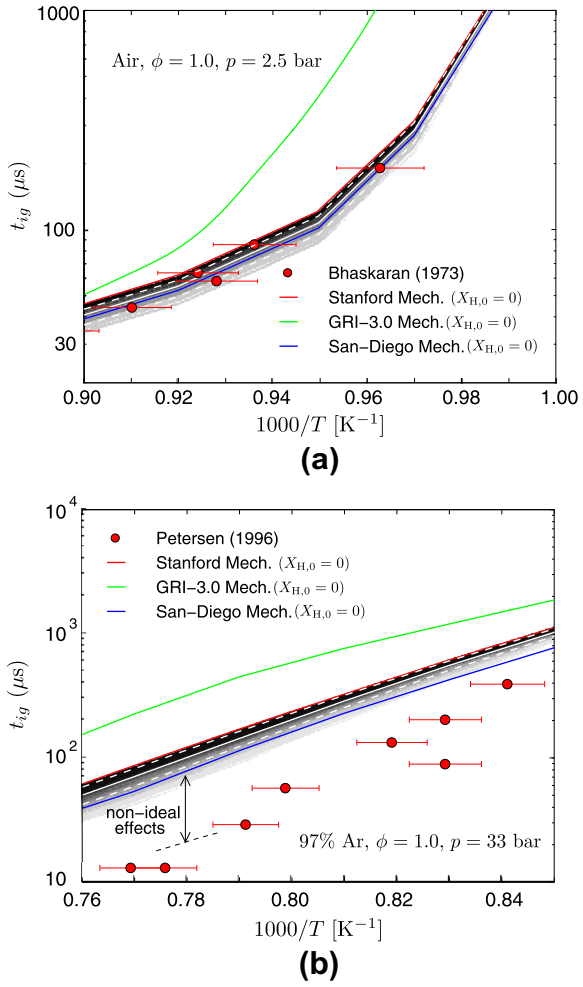


**Fig. 13.** Effects of uncertainties in the residual impurities on the autoignition time (a) near and (b) below crossover. The figure shows PDFs $P(t_{ig})$ after $2 \times 10^5$ simulations, for ignition in air/$H_2$ and (b) $H_2/O_2$/Ar calculated using the Stanford mechanism [2], together with (a) Bhaskaran et al. [36] and (b) Petersen et al. [37] experiments (red dots). Both panels show 1% error bars in temperature around experimental points, the mean E[$t_{ig}$] (solid white line), E[$t_{ig}$] ± standard deviation (dashed white line), and deterministic calculations of $t_{ig}$ calculated with $X_{H,0} = 0$ using the Stanford mechanism (red solid line) [2], the San Diego mechanism (blue solid line) [3] and the GRI v3.0 mechanism (green solid line) [4].

between this branching rate and other rates in the $H_2/O_2$ mechanism. Since the main target of Hong et al. experiments [44] was to determine the branching rate, the experiments were found to be robust in that they were mostly independent of the remaining elementary rates and of the residual impurities in the shock tube.

However, the ramp location in the $H_2O$ concentration time history in Hong et al. experiments [44] is sensitive to the level of impurities, and to the uncertainties in the rates of branching (1f) and – in a lesser extent – initiation (13b), as shown in Fig. 8. That the uncertainties in the rates of (1f) and (13b) are much less important than the level of impurities in the shock tube for the determination of $t_{ig}$ is demonstrated in Sections 4.2 and 4.4. In particular, it is shown in Eq. (16) that a small amount of impurities is typically sufficient for bypassing the initiation stage. In any case, these uncertainties were inconsequential in [44] for the determination of the branching rate because of the procedure used there.

Nonetheless, it should be noted that the measured rates may not always be independent of the level of residual radical impurities in the shock tube if, in particular, the experiments use radical absorption methods, such as O- or H-ARAS [67] and OH-ARAS [50].

Additionally, it is worth mentioning that, in the most general case, the method $\mathcal{M}_2$ of quantification of impurities relies on reference values of rate constants. Since the rate constants of kinetic schemes are not uncertainty-free [51,60,64], the concentration of impurities is subject not only to experimental uncertainties in the determination of the concentration time-histories, but also to uncertainties induced by the inexact chemical rates utilized to retrieve the impurities from experimental signals. The other way around may also be true for specific reaction rates measured with techniques that rely on the absorption of radicals, as mentioned earlier.

Therefore, in the most general case, all uncertainty factors in the experimental variables and in the kinetic parameters may be dependent through a set of equations of the type

$$\mathbf{\Phi}(\mathrm{UF}_{K,1}, \mathrm{UF}_{K,2}, \ldots \mathrm{UF}_{K,M}, \mathrm{UF}_X, \mathrm{UF}_T, \mathrm{UF}_p) = 0, \tag{32}$$

where $\mathbf{\Phi}$ is a problem-dependent operator and the subindices $_K$, $_X$, $_T$ and $_p$ are used to denote kinetic, initial composition, temperature and pressure uncertainty factors. Expression (32) does not account for uncertainties in other kinetic parameters such as activation energy, temperature exponent, collider efficiencies, and fall-off factors. In case that flames are used to isolate rates, additional factors need to be added to (32) in order to treat uncertainties in transport phenomena.

The usual practice in uncertainty-quantification literature in chemical kinetics is to set $\mathrm{UF}_X = \mathrm{UF}_T = \mathrm{UF}_p = 1$, to consider only uncertainties in the pre-exponential factors, and to decouple all $\mathrm{UF}_{Kj}$, $j = 1, \ldots, M$, so that the uncertainties in every kinetic rate are independent and there are no uncertainties in the initial composition, temperature and pressure of the system. Only recent attempts have dealt with cross-correlations in kinetic-rate uncertainties [68,63], including the present study. It should also be noted that, to the best knowledge of the authors, none of the recent treatments have considered any epistemic uncertainties related to model errors in the chemical mechanisms and physical formulations used by numerical simulations to match experimental data.

A general statistical framework useful for analyzing the complex interdependence (32) among different parametric uncertainties in a chemical mechanism, which was referred to as the *active chemical-mechanism approach*, was described elsewhere [64] and will not be pursued here.

## 7. Residual impurities in SCRAMJETS

Propulsion in air-breathing hypersonic airplanes is achieved by the use of supersonic combustion ramjets (SCRAMJETS), in which the oxidizer is supplied at supersonic velocities from the surrounding atmospheric air [69]. The oxidizer stream is mixed and burns in the combustion chamber with the fuel carried onboard. Residual impurities in SCRAMJETS may come from particulates released upon thermal or structural loading on wall materials, by combustion products or by atmospheric entrainment. Whether residual impurities may play a role without any intentional injection during the actual high-altitude flight of a SCRAMJET in the atmosphere still needs to be elucidated and is not the topic of this section.

In ground tests of SCRAMJET engines, the stored high-pressure air stream must be heated considerably in order to simulate the actual hypersonic-flight conditions. The main techniques for achieving air preheating involve the use of electric arcs or the pre-combustion of gases. In the second approach (which is the most economical one), fuel is burnt with air in an auxiliary burner with

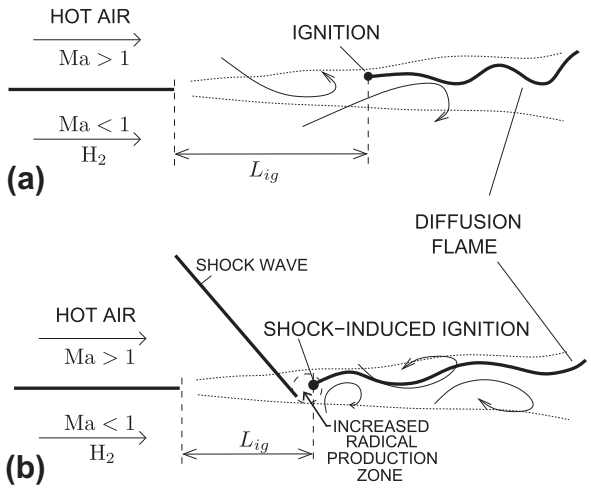


**Fig. 14.** Sketch of two canonical problems often found in SCRAMJET engines: (a) Spontaneous ignition and (b) shock-induced ignition in supersonic mixing layers. Here Ma denotes the Mach number and $L_{ig}$ the distance to ignition.

the resulting products being mixed with oxidizer. The hot vitiated mixture then enters supersonically in the main combustor after being expanded in a convergent–divergent nozzle. At such high velocities, the combustion behavior is found to be extraordinarily sensitive to the inflow composition, which raises concerns about the relevance of ground tests for assessing the engine performance in actual flight conditions, as confirmed by a recent NATO monograph on the topic [70].

In fact, earlier studies [71,72,69,73,74,70] have shown that the presence of active species such as H, O, OH, and $CH_3$ in the inflow gases can accelerate the combustion processes in SCRAMJET engines. The presence of just 10 ppm OH in the combustor inflow assists combustion and can reduce the ignition delay by an order of magnitude [72]. Eq. (23) derived above shows the effects of OH radicals in the autoignition time. In fact, the high benefits of radicals in the inflow of SCRAMJETS can be such that electrical igniters become unnecessary for starting the engine [69,74].

Consider the two canonical configurations often encountered in $H_2$-fueled SCRAMJET engines depicted in Fig. 14. In particular, Fig. 14a shows a mixing layer downstream from a splitter plate separating the fuel from the air stream. In Fig. 14b, the same configuration is shown, but there the mixing layer is impinged by an oblique shock wave caused by a (intentional or unintentional) wall protuberance or by the shock reflection on the combustor wall.

Both scenarios depicted in Fig. 14 have a region far downstream where the chemistry is fast and the influences of impurities shed intentionally would be negligible. In cross-flow SCRAMJETS such as the HyShot-II [75], this region corresponds to a near-equilibrium zone that sits in the bulk of the combustor far from the injector [76]. However, near the splitter plate, and near the fuel injector in the real HyShot-II configuration, there is an ignition region where chemistry is slow and impurities shed intentionally may play a role by shortening the distance to ignition $L_{ig}$ [73,76], in a manner reminiscent of the one described above for the case of a homogenous mixture. It should be noted that a 30 μs variation in the ignition time leads to ∼5 cm variation in $L_{ig}$ at velocities ∼1500 m/s in typical conditions of supersonic combustion.

Similarly, the shock-wave impingement depicted in Fig. 14b enhances flame ignition by a repressurization and mixing-invigoration effect envisioned by Marble [77] and later lab-tested in actual SCRAMJETS [78]. In particular, the production of H and OH radicals is accelerated behind the shock wave, an effect that has been referred to as radical farming [79–81], thereby highlighting the importance of radicals in supersonic-combustion environments.

The deliberate presence of radical impurities through vitiation, shock impingement or other mechanisms such as electric discharge, can accelerate ignition, and shorten $L_{ig}$ in Fig. 14 by way of bypassing the slow initiation step. In practice, this would allow for wider margins of design in another crucial variables such as the combustor inflow profiles. However, thorough studies that may lead to these advantageous control capabilities in SCRAMJETS still remain to be done [70].

## 8. Conclusions

In this study the influences of impurities on the calculation and experimental determination of ignition times in $H_2/O_2$ mixtures were addressed, with particular emphasis on the uncontrolled presence of residual H-atoms in shock tubes. Two methods were proposed for quantifying experimentally the H-residual impurities in shock tubes, namely, a method that consists of detecting OH traces upon shocking initial $O_2$/inert mixtures, and another method in which the amount of impurities is inferred by shortening the delay time calculated after integration of the conservation equations to match autoignition experimental data. The resulting concentrations of impurities could be used to ascertain the H-atom equivalent amount of impurities in standard shock tubes.

Based on experimental data, a stochastic Arrhenius model for the H-impurities was proposed. Using this model, theoretical quantifications of the uncertainties induced by the impurities on autoignition times were performed by using a short 5-step chemistry, which showed that the relative effects of H-impurities delay times above crossover become increasingly large as the dilution increases and as the temperature and pressure decrease, reaching their maximum importance near crossover. A formula was derived that includes the effects of H-impurities on the ignition time. Additionally, a criterion was reported that yields the critical level of impurities above which these have a considerable effect on the ignition time.

For the conditions tested, and according to the short mechanism used here, the effects of chemical-kinetic uncertainties and branching-termination rate correlations on the ignition time were typically negligible compared to the effects of the uncertainties induced by the H-impurities. Exceptions to this conclusion occur at high temperatures in air, for which chemical-kinetic uncertainties dominate.

Below crossover, the effects of the impurities on ignition delay decay rapidly and are negligible compared to the departures produced by the non-ideal pressure-rise effects typically found in shock-tube experiments at such long test times.

Computational quantifications of uncertainties were carried out by using numerical simulations of the homogeneous-ignition problem subject to Monte-Carlo sampling of the concentration of impurities. For the conditions analyzed, these computations show that the variabilities produced in ignition delays by the uncertainties in H-impurities are comparable to the experimental data scatter and to the effects of typical uncertainties of the test temperature when the Stanford chemical mechanism [2] is used. The calculations also show that the utilization of two other different chemical mechanisms, namely San Diego [3] and GRI v3.0 [4], yields variations in the ignition delays which are within the range of the variabilities caused by the H-impurities in the shock tube.

In conclusion, the results obtained in this study suggest that a quantification of radical impurities in the shock tube may be needed prior to undertaking any tuning of the kinetic parameters to match $H_2/O_2$ ignition targets.

Possible extensions of this work could consist of calculating high-speed hydrogen flames under uncertain amounts of residual impurities upon vitiation of the injection port. However, it may be tempting to argue that in realistic situations ignition occurs in turbulent flows – including those depicted in Fig. 14, – and therefore simple analyses based on homogeneous ignition such as Eq. (14) are not relevant due to the absence of strain-rate effects in the formulation. Remarkably, the hydrogen ignition time obtained from homogeneous-ignition analyses tends to be the correct order of magnitude for laminar [82] and turbulent supersonic [83] cases in hydrogen combustion above crossover. In the laminar case, the concentration of radicals diffuses fast across the mixing layer, which tends to homogenize the mixture. In the turbulent case, since the local strain only acts to delay ignition, the mixing zones embedded in the low-strain vortices convected with the flow are the first to undergo ignition [84]. Nevertheless, a thorough assessment of the effects of uncertain amounts of residual impurities in autoignition of turbulent flames would require the use of direct numerical simulations subject to Monte-Carlo sampling of the impurities pool (which may be too costly even at moderately high Reynolds numbers) or the development of new subgrid models of unsteady turbulent combustion compatible with efficient treatments of chemical-composition uncertainties.

A different type of uncertainties not considered in this study are those of the epistemic type, which are related to the observability of the physical processes represented by the homogeneous-ignition model to describe shock-tube experiments. For instance, although shock tubes have been considered over the years to provide a wealth of experimental data under small influences of transport processes, there are situations at long ignition times in which hydrodynamic instabilities can develop in the tube as a result of interactions between the shock wave and boundary layers, which lead to the occurrence of isolated weak-ignition spots that may not be describable by the homogeneous-ignition formulation [85]. The assessment of errors in rate constants and ignition delay times measured in shock tubes may benefit from the simultaneous treatment of all these uncertainties.

## Acknowledgments

This investigation was funded by the Predictive-Science Academic-Alliance Program (PSAAP), DoE Grant # DE-FC52-08NA28614, for investigating uncertainties in hydrogen-fueled SCRAMJETS. The first author was supported by the 2011–2012 Postdoctoral Fellowship for Excellence in Research, Ibercaja Foundation (Zaragoza, Spain).

## Appendix A. Calculation of the global sensitivity $S_j$

For fixed temperature and pressure, the sensitivity index (25) can be approximated by using the following method, which represents a variance decomposition based on a polynomial-chaos expansion of the autoignition time. In particular, consider the expansion

$$t_{ig} = \sum_z u_z \psi_z(\boldsymbol{\beta}), \tag{A.1}$$

where $z$ is a multidimensional index, $u_z$ are the expansion coefficients, $\psi_z$ are multidimensional Hermite polynomials and $\boldsymbol{\beta} = \{\ln \eta_j\}_{j=1}^5$ is a vector of independent standard normal random variables as described in Eq. (11). For a first-order expansion, only the Hermite polynomials $\psi_0 = 1$ and $\psi_1 = \beta$ need to be retained, and (A.1) becomes

$$t_{ig} \simeq \mathrm{E}[t_{ig}] + \sum_{j=1}^5 u_j \beta_j, \tag{A.2}$$

where the coefficients $u_j$ are obtained by multiplying both sides of Eq. (A.2) by $\beta_m \exp\left(-\beta_m^2/2\sigma_{K,m}\right)/(\sqrt{2\pi}\sigma_{K,m})$, integrating the resulting expression with respect to $\beta_m$, and realizing that only the terms $i = m$ are non-zero. In this way, the coefficients

$$u_j = \frac{\mathrm{E}[t_{ig}\beta_j]}{\mathrm{E}[\beta_j^2]} = \frac{1}{\sigma_{K,j}^2 N} \sum_{m=1}^N t_{ig,m}\beta_{j,m}, \tag{A.3}$$

are obtained, with $\sigma_{K,j}$ given in (11) and $N$ being the number of samples per temperature value. Notice that the coefficients $u_z$ are generally dependent on temperature for a fixed pressure, with

$$\mathrm{var}[t_{ig}] = \sum_{j=1}^5 u_j^2 \sigma_{K,j}^2. \tag{A.4}$$

Since the random variables $\beta_j$ are independent, the conditional mean $\mathrm{E}[t_{ig}|k_j]$ can be calculated by using

$$E[t_{ig}|k_j] = E[t_{ig}|\beta_j] \simeq \mathrm{E}[t_{ig}] + u_j\beta_j, \tag{A.5}$$

where use has been made of (A.2). Taking the variance of Eq. (A.5) and using the definition (25), the expression (26) for the global sensitivity $S_j$ is obtained.

## References

[1] G. del Álamo, F.A. Williams, A.L. Sánchez, Combust. Sci. Technol. 176 (2004) 1599–1626.
[2] Z. Hong, D.F. Davidson, R.K. Hanson, Combust. Flame 158 (1) (2011) 633–644.
[3] P. Saxena, F.A. Williams, Combust. Flame 145 (2006) 316–323.
[4] G.P. Smith, D.M. Golden, M. Frenklach, N.W. Moriarty, B. Eiteneer, M. Goldenberg, C.T. Bowman, R.K. Hanson, S. Song, W.C. Gardiner, V.V. Lissianski, Z. Qin, GRI v3.0 Mechanism <http://www.me.berkeley.edu/gri_mech/>.
[5] C.N. Hinshlewood, A.T. Williams, The Reaction Between Hydrogen and Oxygen, Oxford University Press, 1934.
[6] M. Smooke, R.W. Bilger, Reduced Kinetic Mechanisms and Asymptotic Approximations for Methane–Air Flames: A Topical Volume, Springer-Verlag, 1991.
[7] Y. Tan, P. Dagaut, M. Cathonnet, J. Boettner, Combust. Sci. Technol. 102 (1994) 21–55.
[8] M. Frenklach, H. Wang, M. Goldenberg, G.P. Smith, D.M. Golden, C.T. Bowman, R.K. Hanson, W.C. Gardiner, V. Lissanski, An optimized detailed chemical reaction mechanism for methane combustion, Gas Research Institute Topical Report GRI-95/0058, Gas Research Institute, Chicago, 1995.
[9] E. Ranzi, P. Gaffuri, T. Favarelli, P. Dagaut, Combust. Flame. 103 (1995) 91–106.
[10] R.P. Lindstedt, G. Skevis, Combust. Sci. Technol. 125 (1997) 73–137.
[11] M.T. Allen, R.A. Yetter, F.L. Dryer, Combust. Flame 109 (1997) 449–470.
[12] P. Glarborg, M.U. Alzueta, K. Dam-Johansen, J.A. Miller, Combust. Flame 32 (1998) 1–27.
[13] U. Maas, J. Warnatz, Combust. Flame 74 (1988) 53–69.
[14] J.A. Miller, C.T. Bowman, Prog. Energy Combust. Sci. 15 (1989) 287–338.
[15] N. Marinov, C.K. Westbrook, W.J. Pitz, in: S.H. Chan (Ed.), Transport Phenomena in Combustion, vol. 1, 1996, pp. 118–129.
[16] M.A. Mueller, R.A. Yetter, F.L. Dryer, Int. J. Chem. Kinet. 31 (1999) 113–125.
[17] M.O. Conaire, H.J. Curran, J.M. Simmie, W.J. Pitz, C.K. Westbrook, Int. J. Chem. Kinet. 36 (2004) 603–622.
[18] M.P. Burke, M. Chaos, Y. Ju, F.L. Dryer, S.L. Kilippenstein, Int. J. Chem. Kinet. 44 (2012) 444–474.
[19] P. Boivin, C. Jiménez, A.L. Sánchez, F.A. Williams, Proc. Combust. Inst. 33 (2011) 517–523.
[20] K. Seshadri, N. Peters, F.A. Williams, Combust. Flame 96 (1994) 407–427.
[21] D. Fernández-Galisteo, A.L. Sánchez, A. Liñán, F.A. Williams, Combust. Flame 156 (2009) 985–996.
[22] G. Balakrishnan, C. Treviño, F. Mauss, Combust. Flame 91 (1992) 246–256.
[23] G. Balakrishnan, M. Smooke, F.A. Williams, Combust. Flame 102 (1995) 329–340.
[24] B. Lewis, G. von Elbe, Combustion, Flames and Explosions of Gases, Academic Press, 1987.
[25] M. Hattwig, H. Steen (Eds.), Handbook of Explosion Prevention and Protection, Wiley-VCH, 2004.
[26] D.F. Davidson, R.K. Hanson, Int. J. Chem. Kinet. 36 (2004) 510–523.
[27] M. Steinberg, W.E. Kaskan, Proc. Combust. Inst. 5 (1955) 664–672.
[28] G.L. Schott, J.L. Kinsey, J. Chem. Phys. 29 (1958) 1177–1182.
[29] R.A. Strehlow, A. Cohen, Phys. Fluids 5 (1962) 97–101.

[30] S. Fujimoto, Bull. Chem. Soc. Jpn. 36 (1963) 1233–1236.
[31] H. Miyama, T. Takeyama, J. Chem. Phys. 41 (1964) 2287–2290.
[32] T. Asaba, W.C. Gardiner, R.F. Stubbeman, Proc. Combust. Inst. 10 (1965) 295–302.
[33] G.B. Skinner, G.H. Ringrose, J. Chem. Phys. 42 (1965) 2190–2192.
[34] V.V. Voevodsky, R.I. Soloukhin, Proc. Combust. Inst. 10 (1965) 279–283.
[35] T. Just, F. Schmalz, Measurements of ignition delays of hydrogen-air mixtures under simulated conditions of supersonic combustion chambers, AGARD CP No. 34, Part 2, 1968.
[36] K.A. Bhaskaran, M.C. Guptan, T. Just, Combust. Flame 21 (1973) 45–48.
[37] E.L. Petersen, D.F. Davidson, M. Röhring, R.K. Hanson, in: Proceedings 20th Symposium on Shock Waves, 1996, pp. 941–946.
[38] B.L. Wang, H. Olivier, H. Gronig, Combust. Flame 133 (2003) 96–106.
[39] J.V. Michael, J.W. Sutherland, L.B. Harding, A.F. Wagner, Proc. Combust. Inst. 28 (2000) 1471–1478.
[40] R.W. Bates, D.M. Golden, R.K. Hanson, C.T. Bowman, Phys. Chem. Chem. Phys. 3 (2001) 2337–2342.
[41] Z. Hong, A. Farooq, E.A. Barbour, D.F. Davidson, R.K. Hanson, J. Phys. Chem. A 113 (2009) 12919–12925.
[42] Z. Hong, R.D. Cook, D.F. Davidson, R.K. Hanson, J. Phys. Chem. A 114 (2010) 5718–5727.
[43] Z. Hong, S.S. Vasu, D.F. Davidson, R.K. Hanson, J. Phys. Chem. A 114 (2010) 5520–5525.
[44] Z. Hong, D.F. Davidson, E.A. Barbour, R.K. Hanson, Proc. Combust. Inst. 33 (2011) 309–316.
[45] F.A. Williams, Combustion Theory, Addison-Wesley, 1965.
[46] H. Pitsch, Entwicklung eines Programmpaketes zur Berechnung eindimensionaler Flammen am Beispiel einer Gegenstromdiffusionsflamme. M.Sc. Thesis, RWTH Aachen, Germany, 1993.
[47] K.R. Jackson, M.R. Gruber, T.F. Barhorst, The HIFiRE Flight 2 Experiment: An Overview and Status Update, AIAA paper, AIAA 2009-5029:1-19, 2009.
[48] H. Wang, X. You, A.V. Joshi, S.G. Davis, A. Laskin, F. Egolfopoulos, C.K. Law, USC Mech Version II. High-Temperature Combustion Reaction Model of $H_2$/CO/$C_1$–$C_4$ Compounds <http://ignis.usc.edu/USCMechII.htm>, May 2007.
[49] J.T. Herbon, R.K. Hanson, D.M. Golden, C.T. Bowman, Proc. Combust. Inst. 29 (2002) 1201–1208.
[50] D.F. Davidson, E.L. Petersen, M. Röhrig, R.K. Hanson, C.T. Bowman, Proc. Combust. Inst. 26 (1996) 481–488.
[51] D.L. Baulch, C.T. Bowman, C.J. Cobos, R.A. Cox, Th. Just, J.A. Kerr, M.J. Pilling, D. Stocker, J. Troe, W. Tsang, R.W. Walker, J. Warnatz, J. Phys. Chem. Ref. Data 34 (2005) 757–1399.
[52] R.C. Weast (Ed.), Handbook of Chemistry and Physics, CRC Press, Cleveland, 1976.
[53] E.L. Petersen, A Shock Tube and Diagnostics for Chemistry Measurements at Elevated Pressures with Application to Methane Ignition, Ph.D. Thesis, Stanford University, 1998.
[54] J.T. Herbon, Shock Tube Measurements of $CH_3 + O_2$ Kinetics and the Heat of Formation of the OH Radical, Ph.D. Thesis, Stanford University, 2004.
[55] V. Vasudevan, Shock Tube Measurements of Elementary Oxidation and Decomposition Reactions Important in Combustion Using OH, CH, and NCN Laser Absorption, Ph.D. Thesis, Stanford University, 2007.
[56] H. Li, Near-Infrared Diode Laser Absorption Spectroscopy With Applications to Reactive Systems and Combustion Control, Ph.D. Thesis, Stanford University, 2007.
[57] D.A. Masten, R.K. Hanson, C.T. Bowman, J. Phys. Chem. 94 (1990) 7119–7128.
[58] S.S. Vasu, D.F. Davidson, R.K. Hanson, Energy Fuels 25 (2011) 990–997.
[59] P. Boivin, A.L. Sánchez, F.A. Williams, Combust. Flame 159 (2012) 748–752.
[60] A.A. Konnov, Combust. Flame 152 (2008) 507–528.
[61] M.T. Reagan, H.N. Najm, R.G. Ghanem, Combust. Flame 132 (1) (2003) 544–545.
[62] M.E. Mueller, G. Iaccarino, H. Pitsch, Proc. Combust. Inst. 34 (1) (2012) 1299–1306.
[63] J. Prager, H.N. Najm, K. Sargsyan, C. Safta, W.J. Pitz, Uncertainty quantification of reaction mechanisms accounting for correlations introduced by rate rules and fitted Arrhenius parameters, Combust. Flame http://dx.doi.org/10.1016/j.combustflame.2013.01.008.
[64] J. Urzay, N. Kseib, P.G. Constantine, D.F. Davidson, G. Iaccarino, Uncertainty-Quantifying Models for Chemical-Kinetic Rates, Annual Research Briefs, Center for Turbulence Research, Stanford University/NASA Ames, 1–13, 2013.
[65] C. Treviño, Prog. Astronaut. Aeronaut. 131 (1991) 19–43.
[66] G.A. Pang, D.F. Davidson, R.K. Hanson, Proc. Combust. Inst. 32 (2009) 181–188.
[67] P. Frank, Th. Just, Phys. Chem. 89 (1985) 181–187.
[68] D.A. Sheen, H. Wang, Combust. Flame 158 (2011) 645–656.
[69] E.T. Curran, W.H. Heiser, D.T. Pratt, Annu. Rev. Fluid Mech. 28 (1996) 323–360.
[70] G.L. Pellet, C. Bruno, W. Chinitz, Chapter 4: Air Vitiation Effects on SCRAMJET Combustion Tests, NATO Report RTO-TR-AVT-007-V2, 2006.
[71] I. Da Riva, A. Liñán, E. Fraga, J.L. Urrutia, Diffusion Flames and Supersonic Combustion, Technical Report, Instituto Nacional de Técnica Aeroespacial Esteban Terradas, 1966.
[72] R.B. Edelman, L.J. Spadaccini, J. Spacecraft 6 (1969) 1442–1448.
[73] B. Han, C.J. Sung, M. Nishioka, Combust. Sci. Tech. 176 (2004) 305–330.
[74] T. Mitani, T. Hiraiwa, S. Sato, S. Tomioka, T. Kanda, K. Tani, J. Prop. Power 13 (1997) 634–642.
[75] S.J. Laurence, J.M. Schramm, S. Karl, K. Hannemann, An Experimental Investigation of Steady and Unsteady Combustion Phenomena in the HyShot II Combustor, AIAA paper, 2010, pp. 2011–2310.
[76] J. Urzay, N. Kseib, F. Palacios, J. Larsson, G. Iaccarino, A Stochastic Flamelet Progress-Variable Approach for Numerical Simulations of High-Speed Turbulent Combustion Under Chemical-Kinetic Uncertainties, Annual Research Briefs, Center for Turbulence Research, Stanford University/ NASA Ames, 14–27, 2013.
[77] F.E. Marble, Proc. Combust. Inst. 25 (1994) 1–12.
[78] C. Gruenig, V. Avrashkov, F. Mayinger, J. Propul. Power 16 (2000) 22–28.
[79] P.A. Blythe, A.K. Kapila, M. Short, Proc. Combust. Inst. 32 (2009) 2371–2377.
[80] J.R. McGuire, R.R. Boyce, N.R. Mudford, J. Propul. Power. 24 (2009) 1248–1258.
[81] R.R. Boyce, N.R. Mudford, J.R. McGuire, Shock Waves 22 (2008) 9–21.
[82] A.L. Sánchez, A. Liñán, F.A. Williams, J. Eng. Math. 31 (1997) 119–130.
[83] A.L. Sánchez, E. Fernández-Tarrazo, P. Boivin, A. Liñán, F.A. Williams, C.R. Mecanique 340 (2012) 882–893.
[84] E. Mastorakos, Prog. Energy Combust. Sci. 35 (2009) 57–97.
[85] M. Ihme, Y. Sung, R. Deiterding, Detailed Simulations of Shock-Bifurcation and Ignition of an Argon-Diluted Hydrogen/Oxygen Mixture in a Shock Tube, AIAA Paper 2013-0538, 1–14, 2013.